Virology 452-453 (2014) 175–190

Contents lists available at ScienceDirect

Virology

journal homepage: www.elsevier.com/locate/yviro

mTOR/p70S6K signaling distinguishes routine, maintenance-level autophagy from autophagic cell death during influenza A infection

Emmanuel Datan [a], Alireza Shirazian [a,1], Shawna Benjamin [a,1], Demetrius Matassov [a,2], Antonella Tinari [b], Walter Malorni [c,d], Richard A. Lockshin [a], Adolfo Garcia-Sastre [e,f,g], Zahra Zakeri [a,*]

[a] Department of Biology, Queens College and Graduate Center of the City University of New York, 65-30 Kissena Boulevard, Flushing, NY 11367, USA
[b] Department of Technology and Health, Instituto Superiore di Sanita, Viale Regina Elena 299, 00161 Rome, Italy
[c] Department of Drug Research and Evaluation, Instituto Superiore di Sanita, Viale Regina Elena 299, 00161 Rome, Italy
[d] San Raffaele Institute Sulmona, 67039 L'Aquila, Italy
[e] Department of Microbiology, Division of Infectious Diseases, Mount Sinai School of Medicine, New York, NY 10029, USA
[f] Global Health and Emerging Pathogens Institute, Division of Infectious Diseases, Mount Sinai School of Medicine, New York, NY 10029, USA
[g] Department of Medicine, Division of Infectious Diseases, Mount Sinai School of Medicine, New York, NY 10029, USA

ARTICLE INFO

Article history:
Received 15 October 2013
Returned to author for revisions
22 November 2013
Accepted 13 January 2014
Available online 5 February 2014

Keywords:
Influenza
Cell death
Autophagy
Apoptosis
mTORC1/2
p70S6K
Rapamycin
Torin1

ABSTRACT

Autophagy, a stress response activated in influenza A virus infection helps the cell avoid apoptosis. However, in the absence of apoptosis infected cells undergo vastly expanded autophagy and nevertheless die in the presence of necrostatin but not of autophagy inhibitors. Combinations of inhibitors indicate that the controls of protective and lethal autophagy are different. Infection that triggers apoptosis also triggers canonical autophagy signaling exhibiting transient PI3K and mTORC1 activity. In terminal autophagy phospho-mTOR(Ser2448) is suppressed while mTORC1, PI3K and mTORC2 activities increase. mTORC1 substrate p70S6K becomes highly phosphorylated while its activity, now regulated by mTORC2, is required for LC3-II formation. Inhibition of mTORC2/p70S6K, unlike that of PI3K/mTORC1, blocks expanded autophagy in the absence of apoptosis but not moderate autophagy. Inhibitors of expanded autophagy limit virus reproduction. Thus expanded, lethal autophagy is activated by a signaling mechanism different from autophagy that helps cells survive toxic or stressful episodes.

Introduction

Influenza A virus is a major, worldwide, often lethal pathogen (Taubenberger and Morens, 2008). Influenza A virus infection of epithelial, lung and immune cells unconditionally leads to cell death. Autopsies of deceased influenza-infected individuals reveal influenza A virus in damaged tissue and in proximate immune cells (Gill et al., 2010). Damage in lung tissue had often been conventionally described as necrotic based on the morphology of cells in tissue sections. Although it remains unclear if the necrosis observed during autopsies is primary or secondary, several reports from both in-vivo and in-vitro studies have shown virus induced apoptotic cell death. Since the demonstration of apoptosis in-vivo in the lungs and thymus of influenza A virus infected mice (Mori et al., 1995) and liver, kidney and brain of chicken (Ito et al., 2002) the mainstream view of the mechanism behind the pathology of influenza A virus infection has focused mainly on apoptosis-mediated damage. Moreover, elevated lysosomal activity and an abundance of autophagosomes observed when apoptosis is inhibited suggest the involvement of other death mechanisms during infection (Kim et al., 2006; Yang and Chien 2009; McLean et al., 2009).

Focus on how apoptosis is induced by the virus has resulted in the identification of several viral proteins, such as NS1, NA, PB1-F2 and M2 as mediators of virus-induced apoptosis (Zhang et al., 2010; Chen et al., 2001; Ilyinskii et al., 2008). Host proteins with associated cell death functions (e.g. caspases, VDAC, ANT3, NF-κB, Bcl-2, Bax and Bak) also play important roles during infection (McLean et al., 2009; Nencioni et al., 2009; Zhirnov et al., 1999; Zhirnov and Klenk, 2009; Zamarin et al., 2005; Olsen et al., 1996).

* Corresponding author at: Department of Biology, Queens College and Graduate Center of the City, University of New York, 65-30 Kissena Boulevard, Flushing, NY 11367, USA. Tel.: +1 718 997 3417; fax: +1 718 997 3429.
E-mail address: zahra_zakeri@hotmail.com (Z. Zakeri).
[1] Both authors contributed equally to this work.
[2] Present address: Division of Vaccine Vectors, Profectus BioSciences, Tarrytown, NY 10591, USA.

0042-6822/$ - see front matter © 2014 Elsevier Inc. All rights reserved.
http://dx.doi.org/10.1016/j.virol.2014.01.008

Although the importance of viral and host factors in influenza-induced cell death is well documented, the mechanism of interaction for viral and host proteins is not well understood. PB1-F2 and M2 target the mitochondria through an unknown mechanism eventually disrupting function and activating mitochondria mediated apoptotic signaling (Zamarin et al., 2005; Aweya et al., 2013). Moreover, the control of Bax and Bak levels during infection to ensure nuclear fragmentation and release of viral nucleoprotein–RNA complexes to the cytosol remains unclear (McLean et al., 2009).

Cell fate during stress is decided by the activation of several signaling pathways. Autophagy, a major survival response activated in stressed cells, is a highly conserved process in eukaryotes (Yorimitsu and Klionsky, 2005), and several molecules or complexes can up- or down-regulate autophagy by interacting with members of the autophagy pathway. Induction of autophagy can occur through Class 1 PI3K (PI3K-1) and mammalian target of rapamycin complex 2 (mTORC2) or through mammalian target of rapamycin complex 1 (mTORC1). PI3K-1/mTORC2 signaling phosphorylates Akt in response to extracellular ligands (Jiang and Liu, 2008). Akt then phosphorylates mTOR at Serine 2448 and activates mTORC1 (Sekulic et al., 2000), which inhibits autophagy by targeting autophagy related protein (ATG) 13 (Corradetti and Guan, 2006). In contrast, mTOR can alternatively induce autophagy by activating p70S6K in Drosophila fat bodies (Scott et al., 2004), although this situation remains unexplained. Two viral proteins, Influenza NS1 and M2, have been recently associated with autophagy signaling. NS1 binds to p85β, the regulatory subunit of PI3K (Hale et al., 2006), while M2 keeps autophagy at moderate levels by limiting the degree of lysosome fusion with autophagosomes (Gannage et al., 2009). Autophagy, originally characterized as critical for influenza replication (Zhou et al., 2009), was later identified to limit the apoptotic response to infection without affecting virus reproduction (Gannage et al., 2009). However, elimination of influenza-induced apoptosis does not halt virus-induced cell death; instead, an increase in the autophagic state occurs, thus indicating alternative routes to influenza-mediated cell death (McLean et al., 2009).

Here we show that influenza A virus induces autophagy during infection subsequent to activation of canonical autophagy signaling. This induction occurs as apoptotic signaling and death progresses. When cells are unable to undergo apoptosis, infected cells still die, but they exhibit vastly expanded autophagy with robust lysosome turnover. This alternative cell death is not necroptosis. The increased autophagic state manifests altered autophagy signaling with increased mTORC1 and PI3K/mTORC2 activity and p70S6K phosphorylation; while blocking PI3K, mTORC2 or p70S6K activity prevents lethal autophagy and decreases infectious virus production. Our results indicate an underlying role and mechanism for autophagy during influenza A virus infection. Influenza A virus can still kill cells and reproduce even if apoptosis is impeded.

Results

Influenza A virus infection triggers autophagy

Influenza A virus infection triggers autophagy in various cell types (McLean et al., 2009; Zhou et al., 2009). To understand the mechanism by which influenza A virus induced autophagy is triggered we examined canonical autophagy signaling in influenza A virus (MOI=5) infected MDCK cells, which is a mammalian cell line that is both permissive to infection and able to undergo autophagy. We evaluated autophagy by western blot using anti-LC3 antibody. As shown in Fig. 1A, by 8 hours post infection (HPI), 18 kDa LC3-I

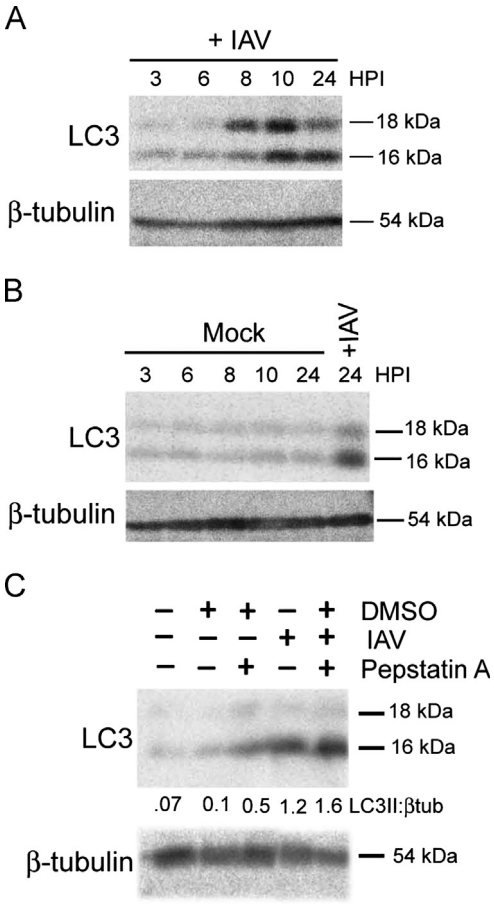

Fig. 1. Influenza A virus activates the autophagy pathway. (A) Upper panel: western blot using whole cell lysates from MOI=5 influenza A infected MDCK cells at 3, 6, 8, 10 and 24 HPI demonstrating the start of 18 kDa LC3-I build-up at 8 HPI, indicating induction of autophagy. 16 kDa LC3-II begins to increase shortly thereafter. (B) This is not observed in mock-infected samples. (C) Exposure of MDCK cells to 10 μg/ml of pepstatin A increases LC3-II relative to β-tubulin (numbers=ratio) in mock-infected and influenza virus infected cells after 24 HPI, indicating that autophagy is functional in both mock-infected (+DMSO+pepstatin A) and infected cells (+DMSO+IAV+pepstatin A). β-tubulin was used as loading control (A–C β-tubulin).

increases dramatically, and reaches a maximum in 10 HPI. We also find a gradual increase in 16 kDa LC3-II, which persists through 24 HPI. These changes are not observed in mock-infected cells (Fig. 1B) and indicate increased autophagy during infection.

Lysosome turnover of autophagosomes, which can be measured by levels of LC3-II after treatment with lysosome inhibitors like pepstatin A, is the hallmark of functional autophagy (Tanida et al., 2005; Mizushima et al., 2010). To determine if increased autophagy during infection is not a result of autophagosome accumulation due to decreased lysosome fusion or function, we assessed LC3-II turnover in lysosomes after exposure of infected cells to the inhibitor of lysosomal cathepsin D, pepstatin A (10 μg/ml), for 24 HPI. Increase in LC3-II resulting from influenza A virus infection was even higher following treatment with pepstatin A, indicating that autolysosomes were turning over, i.e. that they were functional (Fig. 1C LC3). Mock-infection, where cells treated with virus diluting media without virus then given new media, only show low-level autophagosome turn over indicative of housekeeping autophagy (Fig. 1C +DMSO−IAV+pepstatin).

Influenza A infection triggers apoptosis

Influenza A virus kills various types of cells (Taubenberger and Morens, 2008; Gill et al., 2010; Mori et al., 1995; Ito et al., 2002;

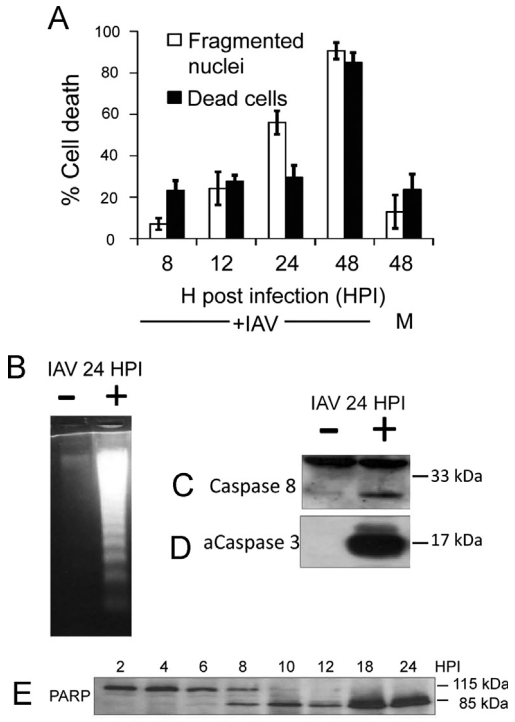

Fig. 2. Influenza infection induces apoptosis through activation of multiple caspases. (A) Using MOI=5 cell death in MDCK cells was assessed at various time points using trypan blue exclusion. Infection with influenza results in 30% death by 24 HPI and most cells die after 48 HPI (black bars). Nuclear fragmentation of infected MDCK cells, as analyzed by the Hoechst assay, also increases with increasing virus exposure until all cells undergo nuclear fragmentation after 48 HPI (white bars). Data shown are means ± S.E. for three independent experiments per sample. Mock-infected MDCK cells have 20% death and nuclear fragmentation after 48 HPI (A, m). Nuclear fragmentation in MDCK cells during infection is coupled with DNA cleavage (B), which is absent in the mock-infected condition (−IAV). Caspase 3 activation (D) and the extrinsic pathway initiator caspase 8 (C) are also activated in infected MDCK cells showing activation of several caspases. Pronounced caspase 3 cleavage of PARP is observed in infected MDCK cells from 8 HPI onwards (E). Uncleaved caspase 8 and cleaved PARP serve as internal loading control (C–E).

McLean et al., 2009; Zhang et al., 2010; Chen et al., 2001; Nencioni et al., 2009; Zamarin et al., 2005; Morris et al., 1999; Mohsin et al., 2002; Wurzer et al., 2003; Wurzer et al., 2004), typically over several days (Fig. 2A). Most of the dying infected cells manifest fragmented nuclei, a characteristic of apoptotic cells while mock-infected cells show minimal cell death and nuclear fragmentation (Fig. 2A, compare +IAV to m). We confirmed death by apoptosis by examining the DNA of infected cells. Unlike mock-infected cells, by 24 HPI infected cells have substantial cleavage of DNA (Fig. 2B). We also found, by western blot, that several caspases, including caspase 3 but also caspase 8, which is normally activated by a cell surface receptor–ligand interaction, are activated (Fig. 2C and D). PARP was also cleaved in a manner typical of caspase-3 (Fig. 2E).

We conclude that, even though autophagy is very active during influenza infection, the vast majority of infected cells undergo apoptosis.

Cell death with increased autophagy occurs after apoptosis is inhibited and is not necroptosis

Inhibition of caspases during exposure to toxins often blocks apoptosis (Lockshin and Zakeri, 2002). To examine the role of apoptosis in influenza-induced death we used caspase 3-deficient MCF7 cells, which are also permissive to influenza A virus as shown by increasing infectious influenza virus production (Fig. 3A right). Consistent with the above results in MDCKs influenza slowly kills MCF7 cells but unlike MDCKs fewer MCF7 cells manifest nuclear fragmentation than membrane permeability (Fig. 3A left). The modest nuclear fragmentation may derive from activation of other caspases by influenza infection (McLean et al., 2009) making caspase 3-deficient MCF7s inappropriate for the study of apoptosis inhibition during infection. To induce a more general caspase blockage we opted for broad acute inhibition of caspases using zVAD-fmk (zVAD).

At 50 μM, pancaspase inhibitor zVAD-fmk completely inhibits activation of caspases 3 and 8 (Fig. 3B and C) in MDCKs even though it only modestly inhibits cell death as measured by trypan blue (Fig. 3D, $^{*}P<0.05$). Virus replication was identical to that seen in the absence of zVAD (Fig. 3F). However as opposed to deficiency of caspase 3 alone in MCF7 cells, zVAD completely blocked virus-induced nuclear fragmentation even at almost 80% cell death (Fig. 3E).

We therefore asked whether the dying cells underwent necroptosis, which can be revealed by inhibition of apoptosis (Degterev et al., 2005). We therefore used an inhibitor to necroptosis, necrostatin (n). As previously shown, zVAD treatment of infected MDCK cells modestly decreases cell death (Fig. 3G compare +IAV– inhib to +IAV+zVAD, $^{*}P<0.05$). Necrostatin at 50 μM did not decrease cell death of infected, caspase-inhibited cells (Fig. 3G, +IAV+zVAD+n50). On the contrary, increasing concentrations of necrostatin to 100 and 200 μM increase cell death in infected, caspase-inhibited (Fig. 3G, compare +IAV+zVAD to +IAV+zVAD+n100 or n200) and uninfected samples (Fig. 3G –IAV+zVAD+n50 to n200). Thus we have no evidence for necroptosis in this system.

Excessive autophagy has also been reported to lead to cell death (Tsujimoto and Shimizu, 2005). This possibility was assessed by morphological examination of MDCK cells through electron microscopy, which indicated the presence of autophagosomes that are considerably larger and more numerous in infected, caspase-inhibited cells (Fig. 3K) than those found in mock-infected, zVAD control or infected cells without zVAD (Fig. 3H, I, and J respectively). Additionally we find by western blot of whole cell lysates from samples identical to those used for electron microscopy that LC3-II is higher when caspases in infected cells are inhibited compared to infection without zVAD (Fig. 3L). Since cell death persists after inhibition of either apoptosis or necroptosis we therefore examined if increased autophagy was sufficient to explain the death of influenza infected caspase-inhibited cells.

Autophagy during alternative mode of death is massive and functional

We blocked autophagy with the inhibitor Wortmannin (20 μm). While this inhibitor alone failed to prevent death of infected cells (Fig. 4A), the combination of the caspase inhibitor zVAD with Wortmannin substantially and significantly (Fig. 4A +IAV+zVAD+wort, $^{***}P<0.005$) decreased the death of infected cells. Even better protection was achieved with increased concentrations of Wortmannin (data not shown). Moreover, cell death in infected ATG 5 KO MEFs with zVAD is lower than in infected ATG 5 wild type with zVAD (Fig. S1, $^{***}P<0.005$). Thus we conclude that vastly expanded (massive) autophagy is a major contributor to the death of caspase-inhibited infected cells.

To characterize autophagy during caspase inhibition, we compared the timing of LC3 activation in infected cells with zVAD to that seen in infected cells where caspases are functional. The kinetics of LC3-I and II are quite different when caspases are inhibited. Unlike infection in the presence of functional caspases, where LC3-I increases by 8 HPI, followed by formation of LC3-II at 10 HPI (Fig. 1A LC3), LC3-I in infected cells with zVAD does not increase while LC3-II very slowly increases (Fig. 4B LC3),

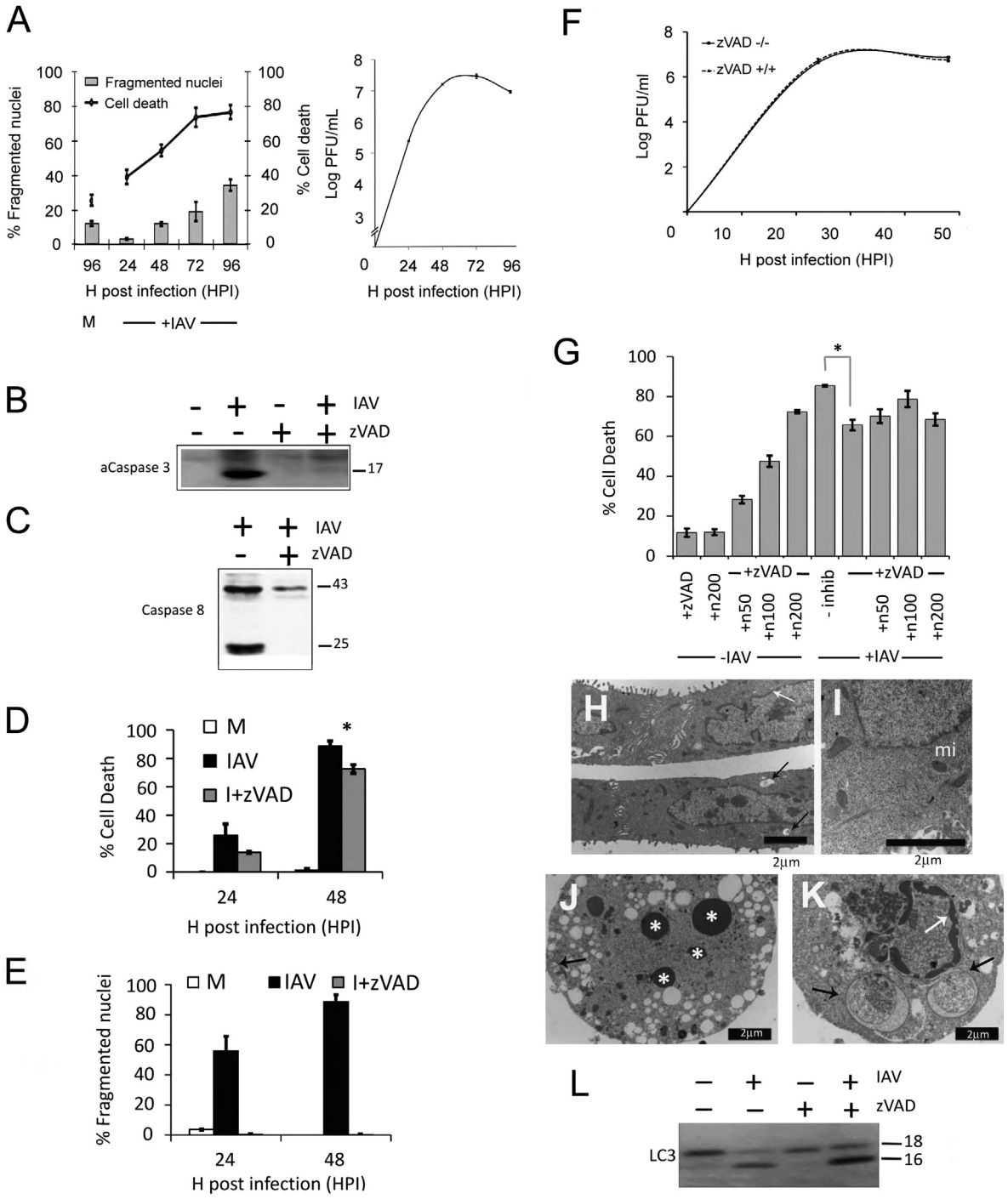

Fig. 3. Broad caspase inhibition blocks influenza induced apoptosis and increases autophagy, but cells still die in a manner independent of programmed necrosis. Cell death and apoptosis during influenza infection (MOI = 5) are not completely absent in caspase 3 deficient MCF7 cells (A left). Infected MCF7 cells allow virus infection and robust infectious virus production (A right). Cell death after 96 HPI in mock-infected MCF7 cells remains low (A, m). However, unlike caspase 3 deficient MCF7, activation of multiple caspases in MOI = 5 infected MDCK cells can be blocked with 50 μM zVAD as shown by the lack of active caspases 3 and 8 after zVAD treatment (B and C). Even 50 μM zVAD inhibition of influenza-induced apoptosis as analyzed by trypan blue (D, $^{*}P < 0.05$) and the Hoechst assay (E) do not prevent death in infected MDCK cells. Mock-infected MDCK cells show minimal cell death (D, m) and nuclear fragmentation (E, m). Inhibition of virus-induced apoptosis in 50 μM zVAD-treated MDCK cells does not affect virus reproduction as measured by plaque assay (F). Treatment of infected, apoptosis-inhibited MDCK cells with 50, 100 or 200 μM of the inhibitor of programmed necrosis necrostatin (n50–200) does not prevent death during apoptosis inhibition (G, $^{*}P < 0.05$). Electron microscopy of samples from mock-infected (H), zVAD control (I), infected cells without zVAD (J) and influenza-infected MDCK cells with zVAD (K). After 24 HPI infected cells without inhibitor show nuclear fragmentation (J, white asterisk) and increased vacuolization (J, black arrow). zVAD prevents influenza induced nuclear fragmentation (K, white arrow) but yields an increase in large autophagosomes (K, black arrows). An intact nuclear membrane (H, white arrow) and few vacuoles in mock-infected cells (H, black arrow) indicate normal physiology. zVAD by itself does not alter cell morphology, as mitochondria (I, mi), and cytoplasm remain normal in zVAD controls. To assess the state of autophagy after apoptosis inhibition we ran whole cell lysates from infected MDCK cells with or without zVAD using SDS-PAGE and performed western blot. We confirm an increase in autophagy after 24 HPI, as shown by LC3-II, in zVAD-exposed infected cells compared to uninhibited infected cells or mock-infected and zVAD controls (L). Data for cell death, fragmentation and titers for MCF7 and MDCK cells were means ± S.E. of three independent experiments.

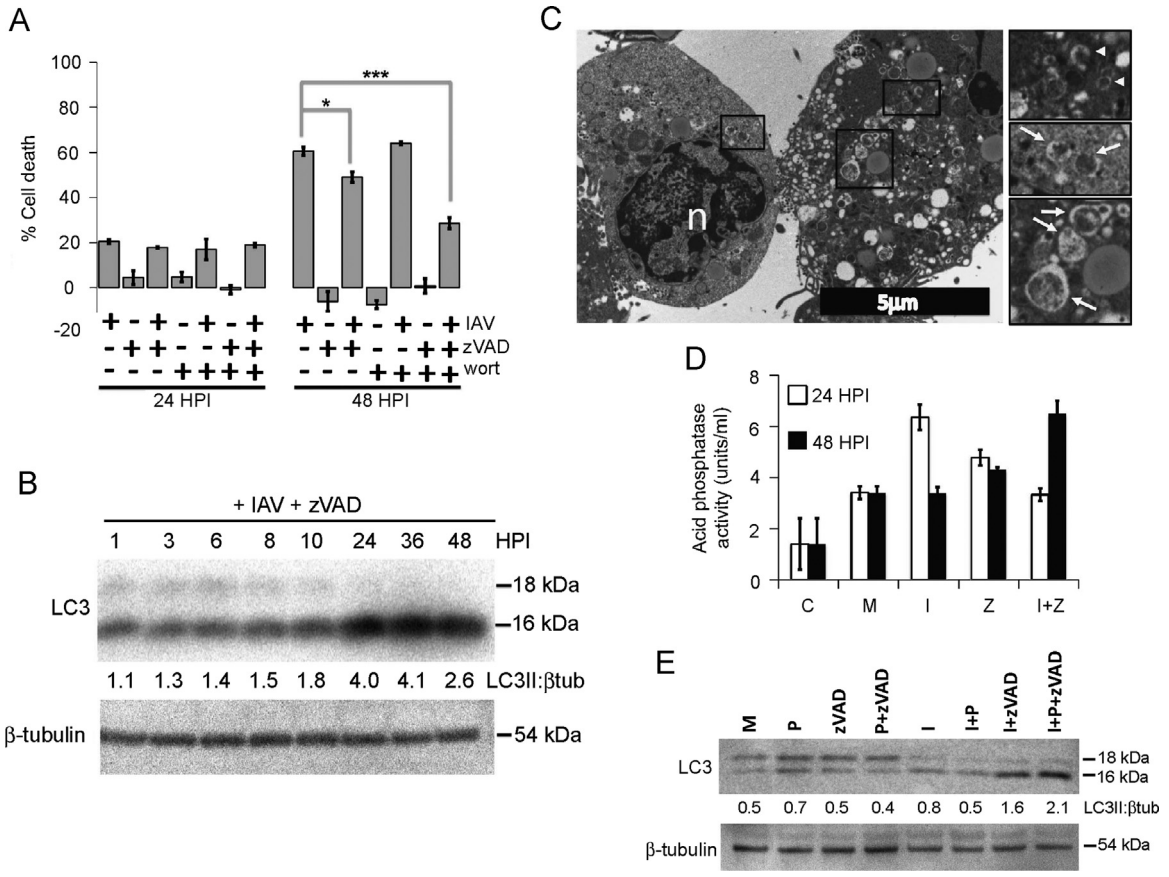

Fig. 4. Massive autophagy in the absence of apoptosis is functional and lethal. (A) Inhibition of autophagy in zVAD-treated, infected cells with 20 μM PI3K inhibitor Wortmannin (wort) decreases virus-induced death in MDCK cells by 48 HPI ($^{*}P<0.05$, $^{***}P<0.005$) although some of infected cells still die in an alternative pathway. Experiments were done in triplicates and data shown are means ± S.E. for each sample. (B) Western blot using whole cell lysates from zVAD-exposed, infected MDCK cells reveals increased autophagy at 24–36 HPI, gradually decreasing at 48 HPI relative to β-tubulin (numbers=ratio). Samples from the experiments in Fig. 3H–K with 24 HPI exposure to zVAD and influenza were fixed for qualitative examination by electron microscopy of autophagosome degradation. Most vacuoles in caspase-inhibited, infected MDCK cells resemble autophagosomes at various stages of degradation (C right: top, middle and bottom). Right panels of (C) represent enlargements of boxed areas displaying: early (C right top, white arrowhead), middle (C right middle, white arrow) and late (C right bottom, white arrow) autophagosomes, which abound in zVAD-exposed infected cells. Lysosome activity in infected MDCK cells as measured by acid phosphatase, a lysosomal enzyme, doubles after influenza infection (i) at 24 HPI (D) compared to controls (c) and mock infected samples (m). Exposure to zVAD during infection (i+z) delays activation of lysosomes similar to infection alone (i) from 24 to 48 HPI independent of zVAD treatment alone (z). One unit of acid phosphatase activity=1 mM freed 4 nitrophenylphosphate min^{-1} mL^{-1} and data shown are means ± S.E. of experiments done in triplicate. Treatment of infected MDCK cells with pepstatin A (p) increases LC3-II, indicating turnover of autophagosomes during infection with zVAD (i+p+zVAD) compared to infection alone with or without pepstatin (i and i+p) or controls (m=mock-infected, p, zVAD, p+zVAD) after 48 HPI (E LC3). Numbers below blots represent ratios relative to β-tubulin (LC3II: β-tub).

suggesting immediate conversion of LC3-I to LC3-II. LC3-II sharply increases at 24 HPI and persists, though declining slowly, through 48 HPI. Infected cells exposed to zVAD contain numerous autophagosomes at various stages of maturity (Fig. 4C: left: overview, right top: early, right middle: middle, and right bottom: late) demonstrating normal autophagosome formation and turnover to lysosomes. As measured by acid phosphatase, lysosomes are functional but activated later in influenza infection with zVAD (Fig. 4D, I+Z) compared to infection without the caspase inhibitor (Fig. 4D, I). Furthermore, inhibition of cathepsin D by pepstatin A (10 μg/ml) leads to accumulation of LC3-II (Fig. 4E LC3) indicating that autophagosomes fuse with lysosomes for degradation (Tanida et al., 2005; Mizushima et al., 2010). Thus when apoptosis is blocked in infected cells, autophagy remains functional and its massive increase is a major component in the eventual death of cells.

Massive autophagy during alternative death depends on modified autophagy signaling

Cell stress triggers autophagy through PI3K and mTOR signaling. Inhibition of PI3K prevents autophagy, while inhibition or knockdown/knockout of mTOR increases autophagy (Scott et al., 2004; Ravikumar et al., 2010). We therefore examined the signaling pathways that lead to induction of massive autophagy when zVAD is present in infected cells. To do this we compared signaling processes when autophagy is provoked by infection in the presence or absence of inhibition of apoptosis. Since Wortmannin targets PI3 kinase, a first step in autophagy signaling, we examined the effect of Wortmannin on LC3 translocation and cleavage. Wortmannin when added during infection alone blocks translocation of LC3 from cytoplasm to autophagosomes, as demonstrated by the failure of formation of puncta (Fig. 5A, compare c to b and quantitation in Fig. 5Af, compare IAV to IAV+W) and accumulation of LC3-II (Fig. 5B and C LC3, compare IAV to IAV+wort 20–40 μM). However, Wortmannin cannot completely block massive autophagy when apoptosis is inhibited by zVAD. GFP-LC3 punctation is still maintained (Fig. 5Ae and Af, compare IAV+Z to IAV+Z+W) and we see conversion of LC3-I to LC3-II by western blot (Fig. 5B and C LC3, +IAV+zVAD+wort). Under these circumstances we find, as expected, active caspase 3 in infected cells without zVAD (Fig. 5B aCaspase3+IAV) and no detected active caspase 3 in mock-infected, treatment controls and infected cells with apoptosis inhibitor (Fig. 5B aCaspase 3, –IAV, +zVAD, +wort,

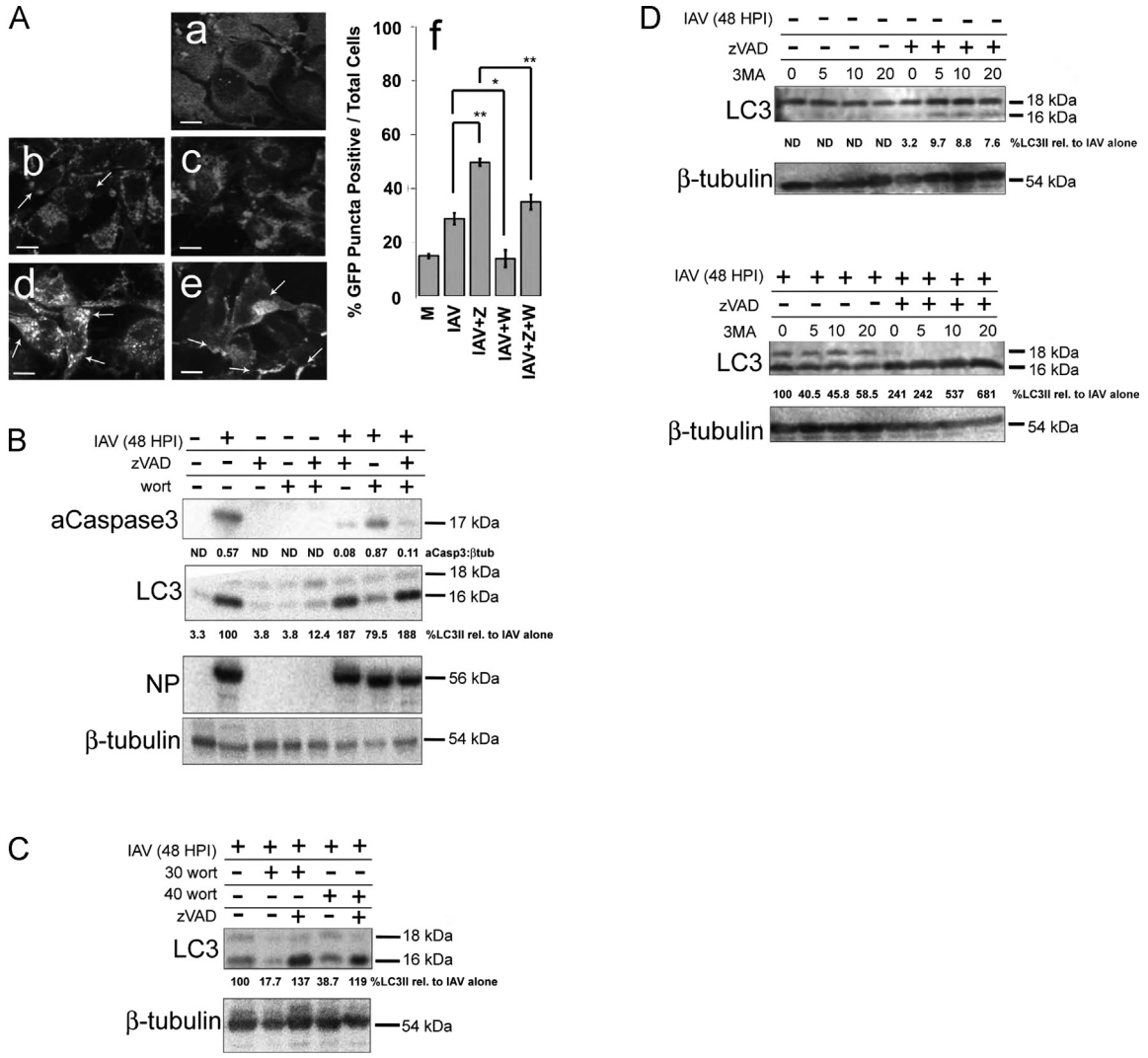

Fig. 5. Massive autophagy relies on alternative autophagy signaling. Punctation of GFP-LC3, a measure of autophagy, was assessed following inhibition of PI3K by Wortmannin. Mock-infected cells (Aa and Af, m) transfected with GFP-LC3 have diffuse GFP-LC3 while infection leads to punctation (Ab, white arrow and Af, IAV). Wortmannin blocks virus triggered punctation (Ac and Af compare IAV to IAV+W, $^{*}P<0.05$) but not in the presence of zVAD (Ae) where punctation persists (white arrows). Treatment with Wortmannin decreases the number of cells with puncta observed in infected cells exposed to zVAD (Ae and Af compare IAV+Z to IAV+Z+W, $^{**}P<0.01$) compared to infection with zVAD alone (Ad, white arrow). (B) Examination of whole cell lysates using SDS-PAGE and antibody against LC3 (B LC3) confirms results from GFP-LC3 cytochemistry. Increasing Wortmannin from 20 μM to 30 and 40 μM leads to substantial decrease of LC3-II in infected cells with apoptosis but only moderately in zVAD-exposed infected cells (C LC3). Wortmannin does not prevent zVAD from blocking virus-induced activation of caspase 3 (B aCaspase 3). Increased caspase 3, when adjusted to protein loading, is observed in Wortmannin treated infected cells (B aCaspase 3, IAV+20 wort). Treatment with 5–20 mM 3MA (3MA 5–20) shows that inhibition of class 3 PI3K by 3MA can also effectively prevent autophagy during infection by itself but not during influenza-zVAD treatment (D LC3, bottom), as is the case with Wortmannin. NP was used as infection control (B NP) while β-tubulin for loading (B–D β-tubulin). Numbers below blots represent ratios relative to β-tubulin.

+IAV+zVAD). Inhibition of autophagy in infected cells without zVAD increased active caspase 3 relative to β-tubulin (Fig. 5B aCaspase 3, +IAV+wort) suggesting a role for autophagy in limiting the apoptotic response to infection. Viral nucleoprotein synthesis was not changed under any of these conditions (Fig. 5B NP). Our findings with Wortmannin are similar to those observed with class 3 PI3K and autophagy inhibitor 3MA where inhibition is most pronounced in infection alone compared to influenza-zVAD treatment (Fig. 5D LC3, bottom).

To further distinguish autophagy regulation in influenza-zVAD treated cells from influenza treatment alone we evaluated the role of mTOR in both situations. To do this we assessed mTORC1 activation through mTOR phosphorylation at Ser2448 (p-mTOR) and activity by levels of phospho-p70S6K (Ravikumar et al., 2010). To fully assess the role of mTOR during influenza infection we also examined mTORC2 activity through phospho-Akt (p-Akt), which PI3K also activates (Jiang and Liu, 2008; Ravikumar et al., 2010). Treatment with zVAD by itself induces a modest level of p-Akt from 1 to 6 HPI that gradually wanes by 10 HPI (Fig. 6A p-Akt, +zVAD). No upregulation of p-mTOR is observed in zVAD treatment control compared to mock-infected cells, which we treat with virus media without virus then give new media as an equivalent to 0 HPI or uninfected cells (Fig. 6A p-mTOR, +zVAD compared to m). Treatment with zVAD increases the level of phospho-p70S6K (p-p70S6K) compared to mock-infected samples (Fig. 6A p-p70S6K, +zVAD compared to m).

Infected cells exposed to zVAD show an early increase in p-Akt at Serine 473 after 3 HPI lasting until 10 HPI (Fig. 6B p-Akt) suggesting increased mTORC2/PI3K activity compared to influenza treatment alone. Influenza infection by itself, as shown in Fig. 6C, transiently increases p-Akt after 6 HPI (Fig. 6C p-Akt). This phosphorylation eventually decreases as autophagosomes are formed from 8 HPI onwards (Fig. 6C LC3). Total Akt in mock-infected, zVAD treatment by itself and infection with zVAD does not change (Fig. 6A and B Akt) compared to infection treatment alone where Akt increases through at least 10 HPI (Fig. 6C Akt).

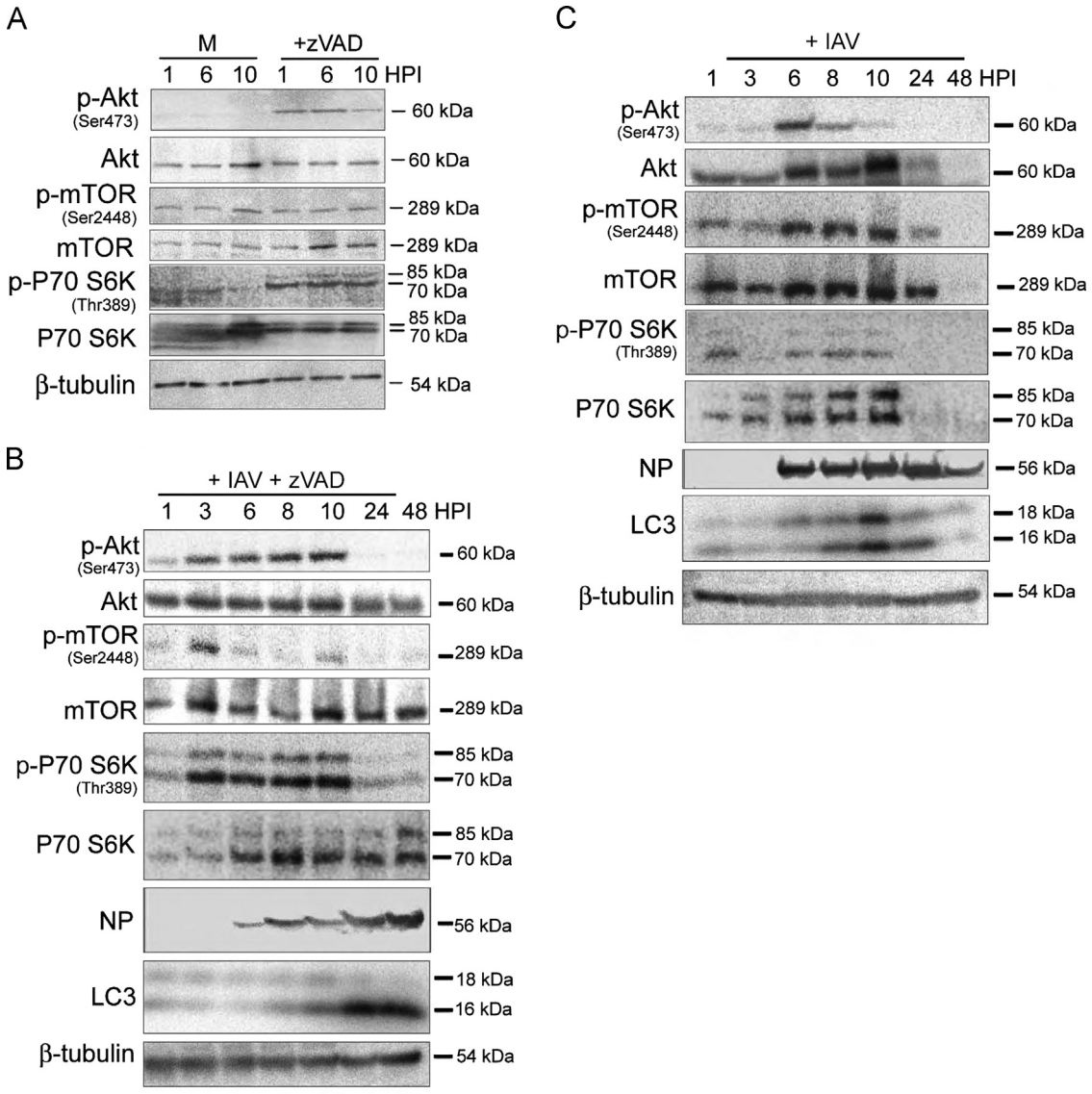

Fig. 6. Altered mTOR/p70S6K signaling occurs during massive autophagy. To identify critical alterations in autophagy signaling responsible for massive autophagy during MOI=5 infection with zVAD we re-evaluated markers for PI3K and mTOR activity at various time points by western blot. No increased PI3K/mTORC2 activity (A p-Akt, M), mTORC1 activation (A p-mTOR, M) or activity (A p-p70S6K, M) is observed in mock-infected MDCK samples. Changes in PI3K/Akt and mTOR signaling are observed during massive autophagy. PI3K/mTORC2 activity is early and prolonged during massive autophagy (B p-Akt). Rapid phosphorylation after 3 HPI is observed in mTOR (B p-mTOR) while phosphorylation of mTOR substrate p70S6K (B p-p70S6K) differs from that seen in infected without zVAD (C p-p70S6K), mock-infected and zVAD controls (A p-p70S6K, M and +zVAD). Although zVAD controls show PI3K/mTORC2 activity and modifications in mTOR substrate phosphorylation, the absence of autophagy in zVAD controls indicates these changes to be sub-threshold (A p-Akt and p-p70S6K, +zVAD). NP shows successful infection (B and C NP) while Akt and p70S6K served as mTOR complex substrate controls. β-tubulin was used for loading control (A–C β-tubulin).

This brief increase of mTORC2/PI3K activity, as shown by p-Akt, in infection without zVAD indicates an upstream role for mTORC2/PI3K in autophagy signaling during influenza A virus infection, which is well underway as shown by expression of virus nucleoprotein starting at 6 HPI (Fig. 6C NP). However, unlike infection by itself p-Akt is increased and sustained during infection with zVAD. We therefore examined the involvement of mTORC1, which can affect levels of p-Akt through feedback (Ravikumar et al., 2010), in the induction of massive, lethal autophagy during influenza-zVAD treatment by examining mTORC1 activation and activity.

The activation of mTORC1, as shown by phosphorylation of mTOR at Serine 2448 and observed in infected MDCK cells from 6 to 10 HPI (Fig. 6C p-mTOR), is not the same as what we find during infection when caspases are inhibited (Fig. 6B p-mTOR). When samples are normalized for protein loading we find substantial p-mTOR at 3 HPI, which is then downregulated to undetectable levels by 24 HPI, at which time we see substantial LC3-II levels (Fig. 6B LC3). Total mTOR remains essentially stable in all conditions (Fig. 6A–C mTOR). Surprisingly, the dephosphorylation of mTOR at Ser2448 (thus deactivation of mTORC1 in infection with zVAD) does not correlate with increased phosphorylation of p70S6K (p-p70S6K) at Threonine 389, a target of mTORC1, compared to infection without zVAD (compare Fig. 6B to C p-p70S6K). Total p70S6K levels remain stable for both influenza alone and influenza-zVAD treatments (Fig. 6A and B p70S6K).

To determine the state of mTORC1 activity during infection with zVAD we re-examined mTORC1 mediated phosphorylation of p70S6K at 10 HPI in infected, zVAD-treated cells after inhibition of mTORC1. Treatment with rapamycin at 50 nM or torin1 at 2 nM inhibits mTORC1 (Liu et al., 2010; Feldman et al., 2009). Rapamycin inhibits p-p70S6K during influenza-zVAD treatment and in infection alone (Fig. 7A p-p70S6K, IAV+Z+R and IAV+R). Low-level

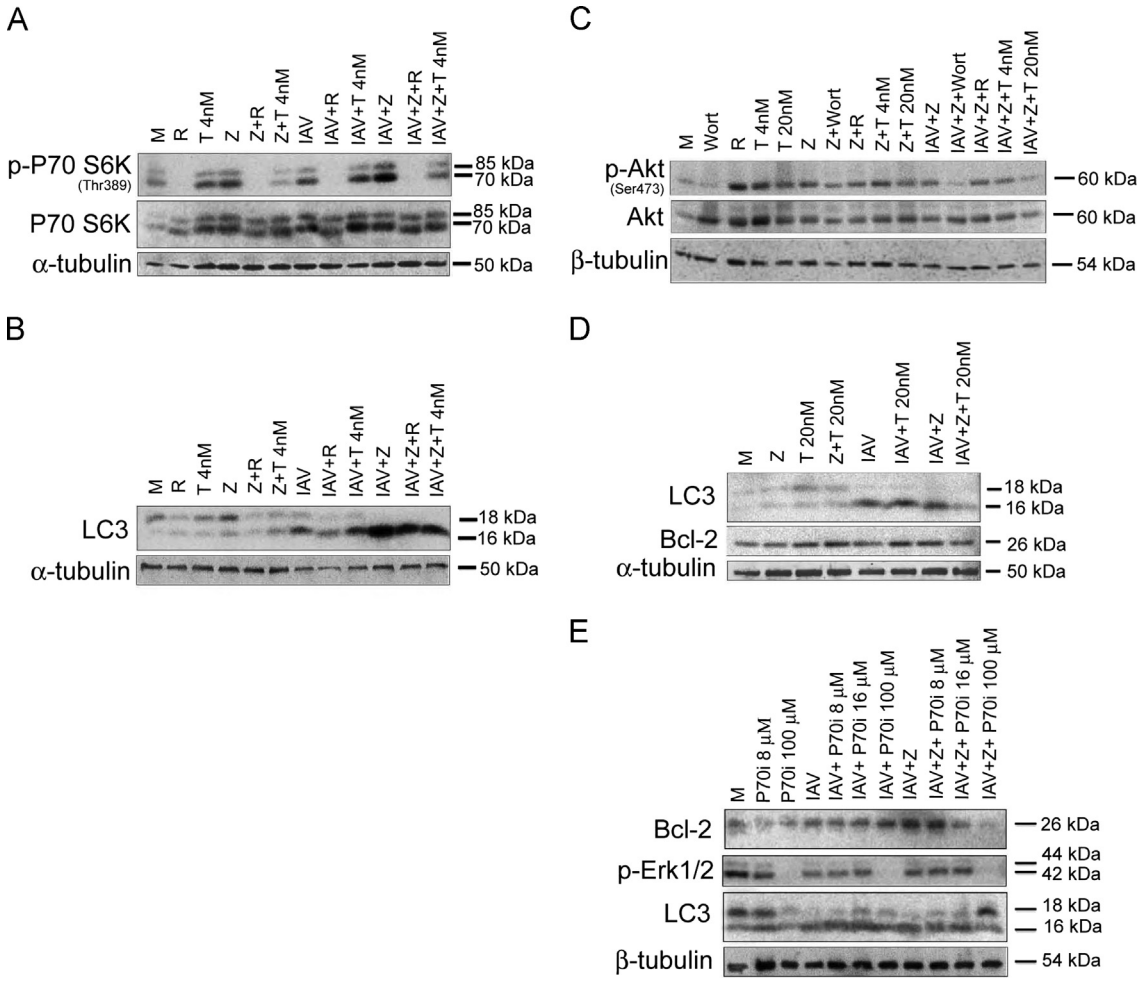

Fig. 7. Massive autophagy requires mTOR/p70S6K activity. Inhibition of mTOR complexes or p70S6K and consequence on lethal autophagy was determined by western blot using whole cell lysates from treatments with mTOR inhibitors. Treatment with 50 nM rapamycin (R) or 4 nM torin1 (T 4nM) inhibits robust mTORC1-mediated p70S6K T389 phosphorylation at 10 HPI (A p-p70S6K) but not expanded, lethal autophagy at 24 HPI (B LC3). PI3K/mTORC2 activity at 10 HPI persists after mTORC1 inhibition (C p-Akt, IAV+Z+R or IAV+Z+T4nM) while treatment with 20 μM PI3K inhibitor Wortmannin (Wort) and mTORC2 inhibitor 20 nM torin1 (T 20nM) inhibited PI3K/mTORC2 mediated Akt phosphorylation (C p-Akt). Inhibition of mTORC2 effectively reduces lethal autophagy (D LC3, IAV+Z+T20nM) and p70S6K activity at 24 HPI as estimated by Bcl2 levels during influenza-zVAD treatment (D Bcl-2, IAV+Z+T20 nM). p70S6K activity inhibitor bis-indolylmaleimide V (P70i) prevents LC3-I conversion to LC3-II only during massive autophagy (E LC3, IAV+Z+P70i 100 μM). This outcome is independent of PKC inhibition (see Results) since the loss of p-Erk1/2 at 100 μM never results in LC3-I build up in treatment control and in apoptosis-competent infected cells (E LC3, P70i 100 μM and IAV+P70i 100 μM). α or β-tubulin was used for loading control (A–E α or β-tubulin).

p-p70S6K in mock-infected cells and increased p-p70S6K by zVAD treatment alone are also blocked by rapamycin (Fig. 7A p-p70S6K, R and Z+R). To ensure inhibition by torin1 we used 4 nM during mTORC1 inhibition and found that 4 nM torin1 inhibits only in the presence of zVAD. Increased p-p70S6K in infected, zVAD-treated cells is lowered by 4 nM torin1 compared to torin1 treatment in infection alone (Fig. 7A p-p70S6K, compare IAV+Z+T to IAV+T). Torin1 also decreased p-p70S6K in zVAD control (Fig. 7A p-p70S6K, Z+T). Total p70S6K increases with treatments and remains stable compared to mock-infected cells (Fig. 7A p70S6K, compare all to M). The inhibition of p-p70S6K by mTORC1 inhibitors rapamycin and torin1 during infection with zVAD shows that mTORC1 is active when influenza-induced autophagy expands. As previously mentioned, to examine whether mTORC1 is part of the regulatory signals controlling expanded autophagy during influenza-zVAD treatment, we examined LC3 levels at 24 HPI after mTORC1 inhibition. Rapamycin or torin1 partially decrease LC3-II, thus inhibit autophagy, during influenza-zVAD treatment (Fig. 7B LC3, IAV+Z compared to IAV+Z+R or IAV+Z+T4nM). Correcting for loading, no inhibition is observed in infection alone (Fig. 7B LC3, IAV compared to IAV+R or IAV+T4nM). This shows that increased mTORC1 activity observed during influenza-zVAD treatment, regardless of Ser2448 phosphorylation on mTOR, contributes the expansion of influenza-induced autophagy. However, mTORC1 inhibition leads only to partial inhibition of expanded autophagy suggesting the involvement of other regulators.

To examine the nature of increased Akt phosphorylation at Ser473 (p-Akt) during expanded autophagy we examined the effect of known upstream Akt kinases mTORC1 and mTORC2 on p-Akt (Ravikumar et al., 2010). Inhibition of mTORC1 with rapamycin or 4 nM torin1, as shown in Fig. 7A, does not decrease p-Akt in influenza-zVAD treated cells (Fig. 7C pAkt, IAV+Z compared to IAV+Z+R or IAV+Z+T4nM) while mTORC2 inhibition by 20 nM torin1 (Liu et al., 2010) like known p-Akt inhibitor 20 μM Wortmannin successfully decreases p-Akt to mock-infected levels (Fig. 7C pAkt, M compared to IAV+Z+T20nM or IAV+Z+Wort). Total Akt in all treatments is increased and remains stable compared to mock-infected condition (Fig. 7C Akt, all compared to M). The sensitivity of p-Akt to mTORC2 or PI3K inhibitors and the persistence

of Serine 473 phosphorylation on Akt after mTORC1 inhibition show that increased mTORC2 and PI3K activity during influenza-zVAD triggered autophagy is independent of mTORC1 activity, which also increases. Furthermore, inhibition of mTORC2 compared to that of mTORC1 successfully decreases LC3-II, thus autophagy, in influenza-zVAD treated cells (Fig. 7D LC3, IAV+Z compared to IAV+Z+T20nM). Torin1 at 20 nM slightly increased autophagy in infected cells with active mTORC1 (Fig. 7D LC3, IAV+T20nM) suggesting inhibition of mTORC1, which inhibits autophagy.

Although 4 nM of torin1 was as potent as rapamycin in decreasing autophagy in influenza-zVAD treated cells the persistence of p-p70S6K after treatment with 4 nM torin1 raised the possibility of dose-dependent sensitivity of p70S6K phosphorylation to torin1. Since mTORC2 activity is increased during massive autophagy and inhibited by 20 nM torin1 we examined the effect of inhibition of mTORC2 (using torin1) on p70S6K. By estimating the activity of p70S6K through levels of Bcl2 (Pastor et al., 2009) at 24 HPI, torin1 at inhibitory concentrations for mTORC2 decreased Bcl2 only during massive autophagy but not in other conditions (Fig. 7D Bcl2, IAV+Z+T20nM). These results indicate the importance of mTORC1 and mTORC2 in the induction of influenza-zVAD-induced massive autophagy and increased p70S6K activation, but not in induction of moderate autophagy in infection treatment alone. Influenza nucleoprotein (Figs. 6B and C NP) indicated successful infection while β and α-tubulin (Figs. 6 and 7 β or α-tubulin) documented equivalent loading. To summarize, we interpret these results to indicate that massive induction of autophagy after blockage of virus-induced apoptosis in this system may be driven by the mTOR/p70S6K pathway, whereas autophagy induction during infection without zVAD may be independent of mTOR signaling.

p70S6K signaling is needed in massive autophagy

Noting the modifications in autophagy signaling and pronounced p70S6K phosphorylation, we explored the role of p70S6K in influenza-induced autophagy. p70S6K controls the amount of autophagy in Drosophila (Scott et al., 2004). To evaluate the role of increased p70S6K phosphorylation just before massive autophagy in infected, caspase-inhibited mammalian cells we inhibited p70S6K activity with P70 inhibitor (P70i) bis-indolylmaleimide V (Marmy-Conus et al., 2002) and estimated the activity of the kinase by measuring Bcl2 (Pastor et al., 2009). Since more than 100 μM P70i also affects PKC (Lazareno et al., 1998) we also evaluated PKC activity by looking at Erk 1 and 2 phosphorylation (p-Erk1/2) (Setalo et al., 2005). The level of Bcl2 is higher during massive autophagy than in infection alone (Fig. 7E Bcl-2, compare IAV+Z to IAV) suggesting increased p70S6K activity. P70i decreases Bcl2 in treatment controls (Fig. 7E Bcl-2, P70i 8 and 100 μM), especially in cells with massive autophagy but not in infected cells without zVAD (Fig. 7E Bcl-2, IAV+Z+P70i 8–100 μM and IAV+P70i 8–100 μM, respectively) indicating differences in p70S6K activity. Inhibition of p70S6K prevents LC3-I conversion to LC3-II only when autophagy is upregulated by zVAD in infected cells (Fig. 7E LC3). This outcome is independent of PKC inhibition since the loss of p-Erk1/2 at 100 μM P70i (Fig. 7E p-Erk1/2, P70i 100 μM) does not increase LC3-I in treatment control (Fig. 7E LC3, P70i 100 μM) or during infection in the absence of zVAD (Fig. 7E p-Erk1/2 and LC3, IAV+P70i 100 μM). Thus, as in Drosophila, mammalian p70S6K increases autophagy when caspases are inhibited in cells challenged with influenza virus. In this situation, altered autophagy signaling affecting mTORC2 and p70S6K leads to massive autophagy, which is an important component in virus-induced cell death.

Inhibition of expanded, lethal autophagy decreases influenza A virus titer

The reduction of virus replication can mitigate virus-induced cell stress during infection (Levine and Kroemer, 2008). To determine the effects of expanded autophagy inhibitors on virus infection and production we examined intracellular influenza A virus nucleoprotein (NP) levels. Inhibition of autophagy does not prevent infection by virus as shown by NP levels after 24 HPI (Fig. 8A NP). Surprisingly, we observe a drastic effect on NP levels after treatment of P70i during infection by itself and in combination with influenza-zVAD treatment where no NP is detected (Fig. 8A NP, IAV+P70i and IAV+Z+P70i). This absence of NP when p70S6K is inhibited (P70i) may be due to the presence of a 5′ terminal oligopyrimidine (TOP) sequence in the untranslated region of NP that presumptively requires p70S6K-mediated translation (Widjaja et al., 2012). However, this is speculation and we have not addressed the issue here.

To determine if viruses are produced during inhibition of autophagy we infected cells with half-diluted supernatant from each treatment condition and measured NP after 6 HPI since NP expression at low MOI is first observed at this time (Tripathi et al., 2013). We diluted the supernatant to minimize the possibility of residual inhibitors affecting virus protein expression. The level of NP as measured by this assay would provide an estimate of released infectious virus progeny for each condition. To test the sensitivity of this assay we used known amounts of virus on cells. Infection of cells with increasing MOI increases NP after 6 HPI showing the sensitivity of this method to differences in infectious particles (Fig. 8B NP, MOI 0.1–10). Using half diluted supernatants from treatments we observe differences in NP level between infection alone and infection with inhibitors. Classic autophagy inhibitor 3MA at 5 mM slightly decreases NP levels in infected cells without zVAD while torin1 at 20 nM increases NP (Fig. 8B NP, compare IAV to IAV+3 MA or IAV+T20nM). Surprisingly, NP is detected after infection with supernatants from P70i treated cells (Fig. 8B NP, IAV+P70i and IAV+Z+P70i) indicating successful primary infection of P70i treated cells and production of infectious virus even with undetected NP in primary infected cells at 24 HPI. Treatment with zVAD does not change NP level compared to infection alone (IAV) but 3MA with zVAD slightly decreases NP while torin1 at 20 nM (T20) dramatically decreases NP levels in influenza-zVAD treated cells (Fig. 8B NP, compare IAV+Z to IAV+Z+3MA or IAV+Z+T20 nM). Expanded, lethal autophagy inhibitors 20 nM torin1 and 3MA reduce infectious virus release during infection with zVAD while no change is observed after P70i treatment as estimated by our assay using initial NP expression.

Another means of approximating the presence of infectious virus is to examine cytopathology after infection. After infecting cells with half-diluted supernatants and incubating them for 24 HPI, we observe considerable cytopathic effects on cells treated with supernatants from all samples except in influenza-zVAD-torin1 20 nM treatment (Fig. 8C, IZT) again indicating infectious virus production during inhibition of autophagy except in infected cells with zVAD and torin1 20 nM. Furthermore, infectious virus production in primary infected cells after 48 HPI as measured by plaque assay is lowered the most by treatment of influenza-zVAD cells with 20 nM torin1, followed by P70i and 3MA (Fig. 8C graph). Autophagy inhibition by 3MA in infection without zVAD also decreases titers. Since released infectious virus progeny as estimated by NP (Fig. 8B) is consistent with plaque assay titers from influenza-zVAD cells with 20 nM torin1 or 3MA but not after P70i treatment where plaque forming progeny is also on decline, the assay in Fig. 8B appears to measure general infectious progeny but not plaque forming virus. The consistent decrease of virus titer during inhibition of autophagy in zVAD-treated cells indicates that

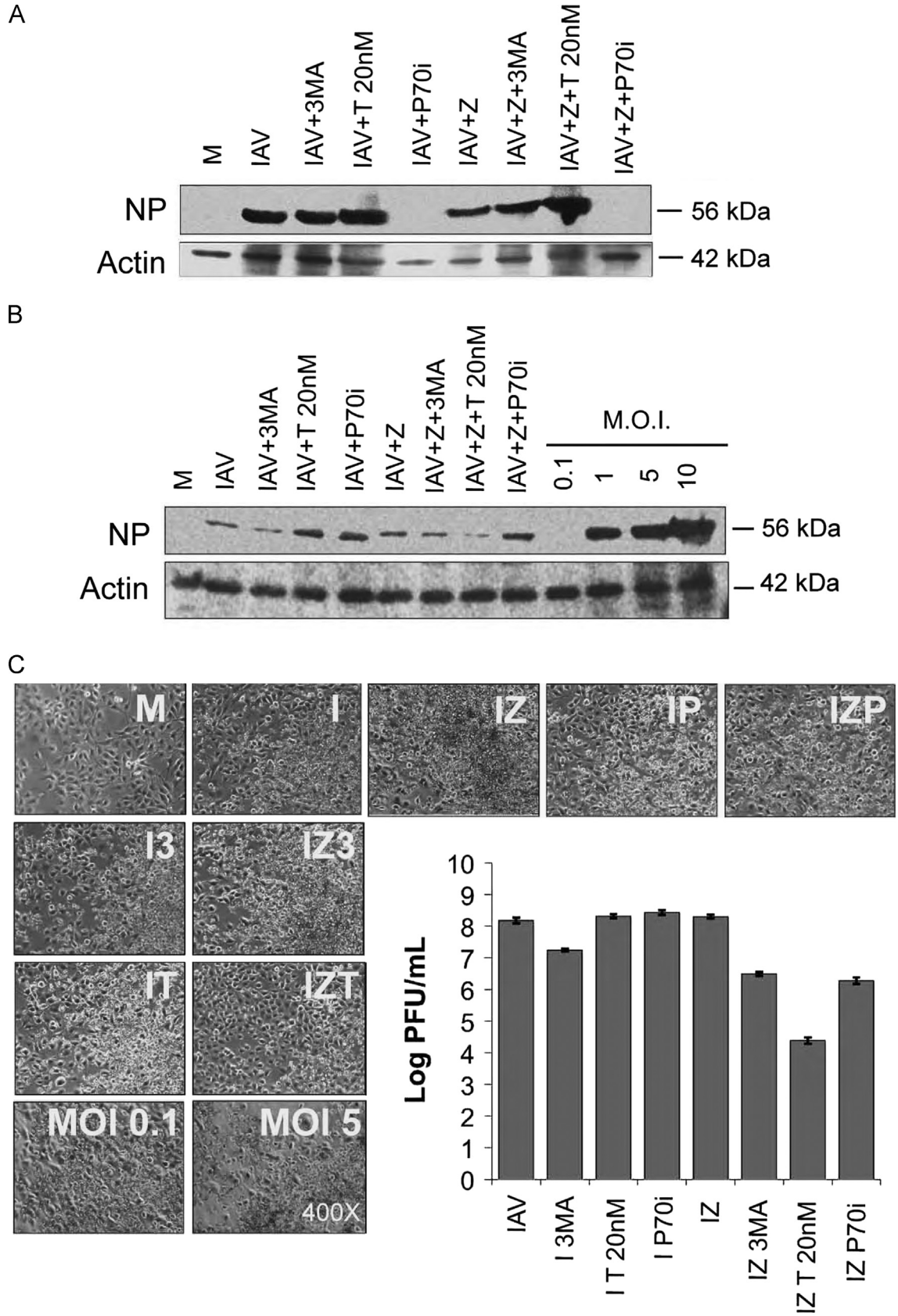

Fig. 8. Inhibition of influenza-zVAD induced autophagy lowers virus production. Autophagy inhibitors 3MA, 20 nM torin1 (T 20 nM) and apoptosis inhibitor zVAD (Z) do not prevent primary infection as shown by western blot of intracellular NP after 24 HPI (A NP). Infection with treatment supernatants, as estimated through NP in cells after 6 HPI, indicates successful primary infection and infectious virus production in all treatments even with undetected NP at 24 HPI (B NP). Levels of NP at 6 HPI vary with increasing influenza multiplicity of infection (MOI) indicating the sensitivity of this assay to differences in infectious particles (B NP, MOI 0.1–10). Treatments with half-diluted supernatants from each treatment condition for 24 HPI all show cytopathic effects except influenza-zVAD-torin1 20 nM (IZT) indicating primary infection and virus production. Plaque assay from supernatants of 48 HPI treated cells show reduction of infectious, plaque forming virus after treatment with apoptosis and autophagy inhibitors (C graph) especially zVAD-torin1 20 nM (IZ T20nM) followed by zVAD-P70i (IZ P70i) and zVAD-3MA (IZ 3MA).

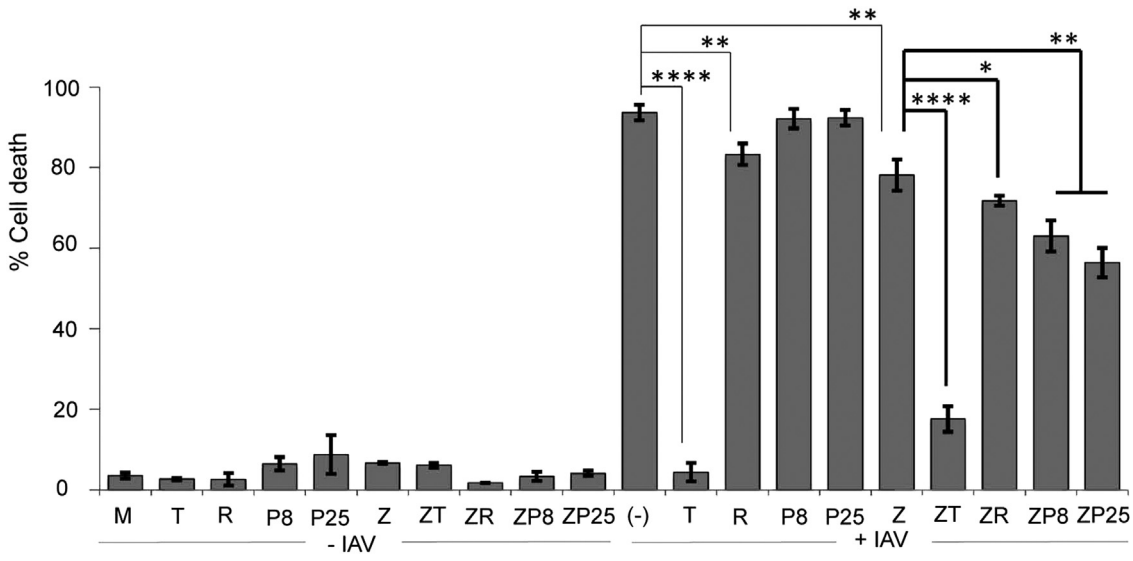

Fig. 9. Inhibition of mTOR/P70 S6K decreases virus-induced death. Cell death assay by trypan blue exclusion after treatment of MDCK cells with 20 nM torin-1 (T) for mTORC1/2, 50 nM rapamycin (R) for mTORC1 or P70i (P8=8 μM, P25=25 μM) for P70 S6K inhibition during MOI 5 infection (+IAV) without or with 50 μM zVAD (Z) after 48 HPI. Mock infection (M) do not show death while infection without inhibitors ((−) +IAV) show high levels of cell death. Asterisks indicate significant differences ($^{*}P<0.05$, $^{**}P<0.01$ and $^{****}P<0.001$).

increased autophagy in the absence of apoptosis contributes to the production of infectious, plaque forming influenza A virus.

Inhibition of mTOR/p70S6K decreases death during lethal autophagy

Inhibition of expanded autophagy by 20 nM torin1 or P70i during infection with zVAD decreases cell death after 48 HPI (Fig. 9) with torin1 conferring more protection than mTOR independent P70i (Fig. 9, compare +IAV+Z to +IAV+Z+T or +IAV+Z+P8/P25). The inhibitors themselves (Fig. 9 −IAV: T, R, P8, P25, Z, ZT, ZR, ZP8, and ZP25) show minimal cell death, similar to mock-infected samples (Fig. 9-IAV M). Surprisingly among other inhibitors, 20 nM torin1 by itself also protects against virus-induced death (+IAV+T) that correlates with increased protective autophagy after 20 nM torin1 treatment (Figs. 7D and S1). Rapamycin by itself, to a lesser extent compared to torin1, also protects against virus-induced death (+IAV+R). These results show that inhibition of expanded autophagy, which occurs during caspase inhibition, using mTOR/P70 S6K inhibitors protects against influenza virus-induced cell death while mTOR inhibition, which increases protective autophagy during apoptosis, limits virus cell killing.

Discussion

Most authors consider that influenza virus activates apoptosis so that it can complete the maturation of virus proteins. The maturation of NP is achieved by caspase activity (Zhirnov et al., 1999; Zhirnov and Klenk, 2009). Extrinsic, as shown by caspase 8 cleavage (Fig. 2C), and intrinsic apoptotic pathways through cytochrome C (McLean et al., 2009) are activated as autophagy increases during infection. However, little is known about autophagy regulation during influenza A virus infection. Here we show that autophagy is induced even as acutely infected cells undergo apoptosis, the default death pathway during infection. As documented here, influenza can also induce massive functional autophagy through alternative signaling involving mTORC1/2 and p70S6K, as can be seen particularly when apoptosis is blocked. Furthermore, we show that virus is still produced during massive autophagy and suppressed the most by the combination of apoptosis–autophagy inhibitors.

Acute infection simultaneously triggers both apoptosis and autophagy while autophagy without cytotoxicity is observed with primary infection using low MOI (Zhou et al., 2009). Influenza A virus-induced autophagy depends on canonical autophagy signaling requiring Beclin-1, ATG 5 and LC3 proteins (Zhou et al., 2009). Presumptively, the low level of autophagy during acute infection (Fig. 1) leads to protection against immediate induction of cell death (Fig. S1); though ultimately influenza infected cells succumb to apoptotic death (Fig. 2). Active caspases and autophagosomes both appear by 8 HPI, and caspase activity continues to increase while autophagy remains low to moderate. Moderate autophagy delays cell death during influenza infection since inhibition of autophagy increases active caspase 3 (Fig. 5B aCaspase 3) and secondary necrosis (Gannage et al., 2009). The role of autophagy in influenza A virus replication during infection with apoptosis is unclear since autophagy deficiency decreases viral RNA (Gannage et al., 2009) and protein (Gannage et al., 2009; Zhou et al., 2009) but have no effect on release of infectious virus (Gannage et al., 2009). Moreover, we show that increased autophagy with lysosome turnover in zVAD-treated infected cells does not affect production of infectious virus (Fig. 3F).

The relationship between virus protein synthesis and autophagy, cell stress and virus production is quite complex as shown by P70i treatment on influenza-infected cells. The drastic effect of P70i on NP has never been described in literature (Fig. 8A). However, the significance of this alteration in virus life cycle and production is too complex to include in this study of autophagy signaling during infection. Here we take the opportunity to present this interesting link between p70S6K and viral protein expression for future studies on host–virus interaction.

The role of autophagy is revealed in the absence of influenza-induced apoptosis where pharmacological inhibition of autophagy, especially by 20 nM torin1 (Fig. 7D), greatly reduces infectious virus progeny but only moderately during infection alone (Fig. 8C graph). The effect of autophagy on infectious virus production may be limited by apoptosis since autophagy expands during infection with zVAD but is induced only moderately in infected cells with apoptosis. Since high level of NP is observed in infected cells with zVAD and 20 nM Torin1 (Fig. 8A NP, IAV+Z+T 20 nM) the decrease in infectious virus after inhibition of autophagy may be due to disruption of infectious particle release from infected cells

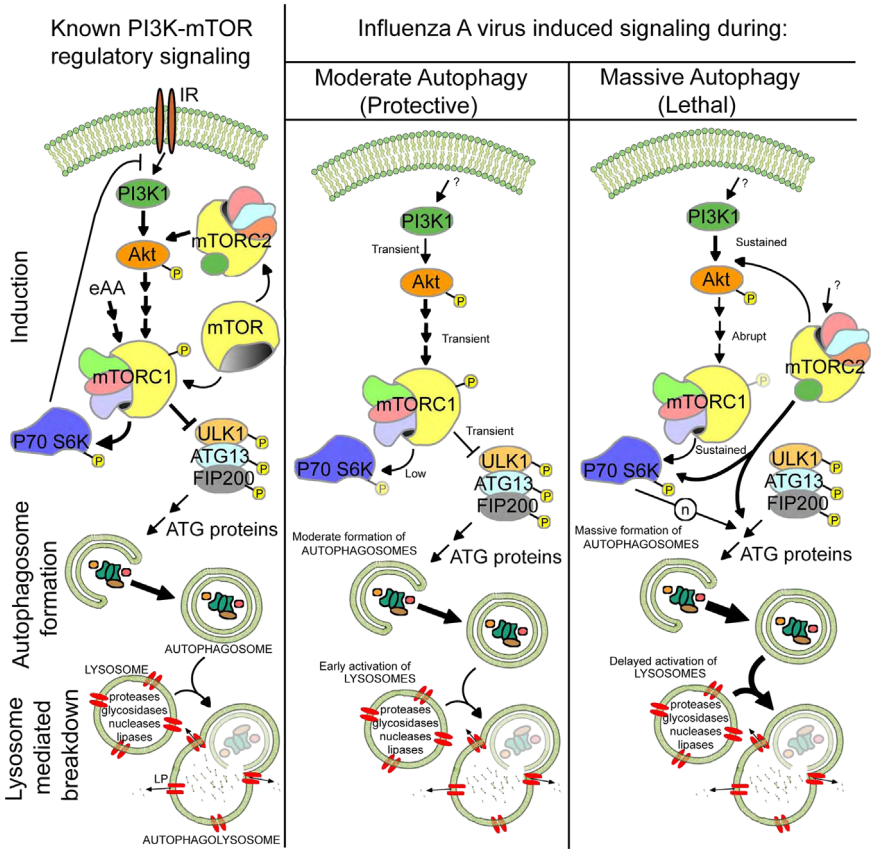

Fig. 10. Regulatory signaling of autophagy during influenza A virus infection. (Left panel) Regulation of autophagy by PI3K and mTOR signaling occur during starvation, hypoxia, or deprivation of insulin or growth factor. Many of the pathways triggered by different inducers converge on mTORC1, an inhibitor of autophagy. mTOR can either form mTORC1 (with Raptor, mLST8, and PRAS40) or mTORC2 (with Rictor, mLST8, SIN1, and PROTOR). The presence of essential amino acids (eAA) during nutrient rich conditions activates mTORC1. Insulin, the mammalian master hormone of the fed state activates PI3K class 1 (PI3K1) through cytoplasmic insulin receptor (IR), which in turn leads to a cascade involving Akt that eventually activates mTORC1. Active mTORC1 prevents ULK1 mediated ULK1–ATG13–FIP200 phosphorylation, which triggers autophagy. PI3K signaling, mTORC1 or Erk can phosphorylate p70S6K. Phosphorylation of p70S6K, which can feed back to PI3K activation, decreases during autophagy. mTORC2 can also activate Akt. Numerous autophagy related proteins or ATGs form complexes for autophagosome formation. Breakdown of engulfed contents by proteases, glycosidases, nucleases and lipases occur through autophagosome fusion with the lysosome. Lysosome permeases (LP) release amino acids, lipids, nucleosides, and carbohydrates back to the cytosol for use in synthetic and metabolic pathways. Protective and lethal autophagy differs in PI3K/mTOR signaling. Transient PI3K activity leading to Akt phosphorylation followed by mTORC1 activation occurs during moderate autophagy (middle panel). Low-level p70S6K phosphorylation is also observed. Autophagy then progresses with increased autophagosome formation and early activation of lysosomes. Massive autophagy (right panel) exhibits increased and prolonged Akt phosphorylation. However, this does not translate to mTOR phosphorylation at Serine 2448 and we only observe transient mTORC1 activation; instead an abrupt activation of mTORC1 is followed by dephosphorylation. mTORC2, which is reported to increase in the absence of mTORC1, compliments PI3K-mediated Akt phosphorylation during massive autophagy. Although mTORC1 lacks Serine 2448, mTORC1-mediated p70S6K phosphorylation still occurs. mTORC2 also contributes to the regulation of p70S6K activity during massive autophagy. In this situation, inhibition of p70S6K activity or mTORC2 prevents massive, lethal autophagy. The number of steps (n) and nature of p70S6K regulation of autophagy remain unknown (see Discussion). Delayed activation of lysosomes is also observed. Viral and host components that trigger these changes are currently being identified.

or production of immature virus. Furthermore, this finding supports the explanation that inhibition of autophagy by torin1 is not an artifact derived from decreased intracellular virus production.

Other regulatory mechanisms control autophagy in influenza-infected cells (Fig. 10). Activation of mTORC1 leads to inhibition of autophagy (Corradetti and Guan, 2006; Ravikumar et al., 2010; Pattingre et al., 2008). Influenza A virus infection activates mTORC1 at 6–10 HPI (Fig. 6C p-mTOR), in conjunction with increase in autophagosomes and caspase activity (Figs. 6C LC3 and 2E PARP). The activation of mTORC1 does not stop caspases from cleaving substrates (e.g. PARP), a critical process in apoptosis. Active mTORC1 phosphorylates various substrates to synchronize catabolic and anabolic processes (Ravikumar et al., 2010; Nicklin et al., 2009). When autophagy is blocked by mTORC1 inhibition of ULK1–ATG 13–FIP200 complex (Corradetti and Guan, 2006), a broad mTORC1 phosphorylation of translation regulators like p70S6K occurs (Ravikumar et al., 2010; Nicklin et al., 2009; Alexander et al., 2010). On the other hand, the phosphorylation of p70S6K decreases during autophagy (Ravikumar et al., 2010). Thus the phosphorylation of mTORC1 substrates, like phosphorylation of mTORC1 itself, can be used as a mark of autophagy inhibition by mTORC1 (Fig. 10 left panel). We observe this increase in phosphorylated mTORC1 with modest phosphorylation of p70S6K during moderate autophagy after infection without zVAD (Fig. 6C p-p70S6K). Treatment of infected cells (i.e. infection with no zVAD) with mTOR inhibitor torin1 at inhibitory concentrations for mTORC2 slightly increases LC3-II (Fig. 7D LC3, IAV+T 20 nM) indicating an effect on mTORC1. Surprisingly, 20 nM torin1 protects against influenza-induced death (Fig. 9 +IAV+T) without inhibiting virus infection and production (Fig. 8). Although mTOR phosphorylation is high at early time points, mTORC1 may not play a dominant inhibitory role on the induction of autophagy in this situation (Fig. 10 middle panel, moderate autophagy) since mTORC1 inhibition with 4 nM torin1 or 50 nM rapamycin did not increase autophagy during infection alone (Fig. 7B LC3, compare IAV to IAV+R or IAV+T 4 nM).

However, when influenza-induced apoptosis is inhibited, autophagy increases massively and leads to cell death (Fig. 4) in an ATG5 dependent manner (Fig. S1). Massive autophagy when apoptosis is inhibited occurs in the absence of mTORC1 activation (Fig. 6B

p-mTOR). Cells undergoing autophagic death have suppressed mTORC1 signaling (Suh et al., 2010). Furthermore, mTORC1 substrate p70S6K, which is robustly phosphorylated at early times in infected, zVAD treated cells, is no longer phosphorylated by 24 HPI (Fig. 6B p-p70S6K) when autophagy is maximized as defined by a sharp increase in LC3-II (Fig. 6B LC3). Although this increase in phosphorylation of p70S6K at Threonine 389 is under mTORC1 regulation (Fig. 7A p-p70S6K) the limited effect of mTORC1 inhibition on lethal autophagy (Fig. 7B LC3), persistent p70S6K phosphorylation after 4 nM torin1 treatment (Fig. 7A p-p70S6K) and reduction of p70S6K activity after mTORC2 inhibition (Fig. 7D Bcl-2) indicate that p70S6K may be targeted by both mTORC1 and mTORC2 during lethal autophagy (Fig. 10 right panel, massive autophagy). The increased level and early kinetics of p-p70S6K during massive autophagy suggests a regulatory role in induction. Thus a non-inhibitory mTOR signaling may be active when influenza-induced apoptosis is inhibited and massive autophagy is induced.

Increased p70S6K phosphorylation is observed with increased p-Akt (Fig. 6B p-Akt). The activation of mTORC1, PI3K, mTORC2 or Erk has been shown to affect p70S6K phosphorylation at Threonine 389, an essential component of p70S6K activity (Vanhaesebroeck and Alessi, 2000; Han et al., 1995). However, constant levels of p-Erk1/2 during massive autophagy (Fig. 7E p-Erk1/2) cannot explain the sustained increase of p-p70S6K at Threonine 389. Furthermore, mTOR phosphorylation at Serine 2448, which activates mTORC1, is suppressed during massive autophagy (Fig. 6B p-mTOR) while PI3K/mTORC2 activity as measured by Akt phosphorylation is increased and correlates with p70S6K phosphorylation (Fig. 6B p-Akt). We observe that mTORC1 still regulates p-p70S6K during influenza-zVAD-induced autophagy (Fig. 7A p-p70S6K). In addition to mTORC1, mTOR in the form of mTORC2 also regulates p70S6K during autophagy (Fig. 7D Bcl-2). Inhibition of mTORC2 by torin1 at 20 nM decreases p70S6K activity and successfully blocks massive autophagy in infected cells with zVAD (Fig. 7D Bcl-2 and LC3) demonstrating an alternative role for mTORC2 as a stimulator of autophagy (Fig. 10 right panel, massive autophagy). Inhibition of lethal autophagy by 20 nM torin1 also correlates with decreased virus-induced death during caspase inhibition (Fig. 9 +IAV+ZT). Furthermore, a more direct inhibition of p70S6K activity with bis-indolylmaleimide V (P70i), an mTOR independent p70S6K inhibitor (Marmy-Conus et al., 2002) prevented LC3-I conversion to LC3-II, a critical process in autophagosome formation, in the situation of massive autophagy (Fig. 7E LC3). Treatment with P70i also decreases cell death during lethal autophagy (Fig. 9). Thus in this situation loss of mTOR Serine 2448 phosphorylation correlates with increased mTORC2 activity and mediated p70S6K activation, suggesting alternate pathways for p70S6K activation that do not require mTOR phosphorylation at Ser 2448 (Fig. 10 right panel, massive autophagy). Since both mTORC2 and p70S6K inhibition effectively inhibit autophagy in influenza-zVAD treated cells these two kinases may belong to a common signaling pathway or affect critical autophagy pathways (Fig. 10 right panel, massive autophagy). The phosphorylation of p70S6K determines the amount of autophagy in Drosophila (Scott et al., 2004), which we also observe in massive autophagy of MDCK cells. Expression of activated Drosophila p70S6K can increase the rate of autophagy in cells experiencing chronic target of rapamycin (TOR) inactivation but not in cells undergoing short-term autophagy (Chang et al., 2009). A subtle difference in autophagy regulation exists between TOR inactivation by truncation and TOR knockout, where TOR inactivation selectively increases autophagy during nutrient rich situations unlike TOR knockout mutants that increase autophagy indiscriminately (Scott et al., 2004). This selective induction by inactive TOR resembles our observation in zVAD treated infected MDCK cells (Fig. 6B p-mTOR and p-p70S6K) where loss of Serine 2448 and not loss of mTORC1 activity correlates with increased p-p70S6K and massive autophagy. Moreover, inhibition of mTORC1 that lack p-mTOR inadequately prevents lethal autophagy unlike direct p70S6K inhibition or mTORC2 inhibition. p70S6K may have autophagy related functions that do not depend on mTORC1-mediated activation at Threonine 389. Thus, it appears that the role of p70S6K during massive autophagy with chronic TOR inactivation is conserved in Drosophila and mammals.

We propose that increased and prolonged autophagy requires the translation of several components of the autophagosome. Critical autophagy proteins increase during autophagy (Wong et al., 2010). Inhibition of protein synthesis disrupts expansion of autophagosomes (Abeliovich et al., 2000) and lysosomal turnover (Lawrence and Brown, 1993). Various autophagy-related proteins (ATG) possess target sequences called 5′ terminal oligopyrimidine tracts (5′ TOP) for p70S6K-mediated translation (Table 1). The presence of this sequence composed of an invariable cytosine succeeded by a stretch of 5–14 pyrimidines (i.e. cytosine and uracil) of mRNA allows S6 ribosome/polyribosome binding and consequent translation of the bound transcript (Levy et al., 1991; Jefferies et al., 1997; Yamashita et al., 2008). The translational control for different 5′ TOP mRNAs is the same regardless of pyrimidine count (Avni et al., 1994). LC3/ATG8, a critical autophagy protein, possesses a 5′ TOP sequence and is highly expressed even in GFP-LC3 form during massive autophagy (Fig. 5Ad). This increased expression of GFP-LC3, the presence of 5′ TOP in several critical autophagy related proteins, and the importance of p70S6K activity in induction of massive autophagy collectively suggest that increased p70S6K activity increases levels of autophagy due to increased ATG translation. We are currently exploring this possibility.

Table 1
Terminal Oligopyrimidine Tract (TOP) in untranslated region of mRNA for various autophagy related proteins.

Protein	Nucleotides before start codon	Sequence
ATG8/LC3	33–25	CUUUUUU
ATG3	43–38	CUUUCC
ATG5	333–328	CUUUUU
	314–309	CUUCCU
ATG7	99–94	CUUCCC
ATG4	442–437	CUCCUU
	414–409	CCUUUU
	339–334	CUUUCU
	323–317	CCUCUUC
	237–230	CUCCUCCU
	160–155	CCUUUU
	145–139	CUCUUCU
ATG10	185–176	CUCUUCCUCC
	97–88	CCCUCUCCCC
	85–73	CUCUCCUCCCCCU
ATG12	81–72	CUCCUCUCCC
ATG16	107–102	CUUUUU
ATG13	626–606	CUCUCUCUCUCUCUCUC
	597–591	CCUUUCC
	429–421	CCCUCUUUC
	419–408	CCCCCCCCCCCC
	222–216	CCCUUCU
	92–87	CUCUUU
	37–32	CCUCCU
UVRAG	188–180	CUCUUCCUU
	112–107	CCUCUC
Ambra1	45–39	CUCCUUC
Bcl-2	455–450	CCUCCU
	441–430	CUCCCUCUCCCC
	134–128	CCCCCUC
	83–68	CUCCUCUUCUUUCUCU
	17–8	CUUUUCCUCU
ATG6/Beclin1	150–142	CUUUUUU
ATG14/Baktor	18–9	CUCUCCUCUC

Data is reproduced from UCSC genome database (Meyer et al., 2013).

Autophagy is completed as autophagosomes fuse with lysosomes to degrade cargo (Corradetti and Guan, 2006; Ravikumar et al., 2010; Pattingre et al., 2008). Increase in autophagosomes during zVAD treatment was previously attributed to lysosome disruption by zVAD that leads to loss of turnover or flux of autophagy (Lockshin and Zakeri, 2002; White, 2008). We show here that delay in lysosome activation, not permanent inhibition of lysosomes, occurs during infection when apoptosis is inhibited by zVAD (Fig. 4D). Lysosome activity is high when autophagy is increased and autophagosomes of different stages of degradation are observed in caspase-inhibited infected cells (Fig. 4C). Delayed lysosome activation when autophagy is increased can lead to buildup of autophagosomes but these autophagosomes remain functional, as documented by turnover of autophagosomes even when autophagy is very high (Fig. 4E), consistent with findings on zVAD-induced autophagy in other cell types (Wu et al., 2008).

To summarize, we demonstrate that the protective and lethal aspects of autophagy can be examined in influenza A virus infected cells. Protective autophagy is characterized by moderate induction with mTOR phosphorylation (i.e. mTORC1 activation) and immediate lysosome activation. In contrast, the absence of mTOR Serine 2448 phosphorylation concomitant with increased mTORC1/mTORC2 mediated p70S6K activity, increased LC3, delayed increase in lysosome activity and exacerbation of autophagosome accumulation typifies massive, unrestrained autophagy.

It may be possible to limit the pathology of influenza A virus infection by simultaneous blockage of apoptosis and autophagy since inhibition of both processes drastically lowers virus production. Instead of focusing only on targeting components of canonical autophagy signaling, inhibition of mTORC2 or p70S6K activity should also be employed in conjunction with other inhibitors. Although we do not observe adverse effects by mTORC2/P70 S6K inhibition and zVAD treatment in our system (Fig. 9), examination of toxicity dose curves on different cell types and in-vivo models would reduce potentially lethal side effects by these inhibitors. For example, prolonged exposure with lower doses of P70i can still decrease cell death during lethal autophagy (Fig. 9) and limit autophagy (data not shown) without being toxic. Moreover, certain cells like those in the preimplantation fertilized ova of mice undergo cell death in the presence of zVAD (Zakeri et al., 2005) emphasizing the importance of toxicity studies. In conclusion, the main mechanism of cell death or loss during influenza A virus infection is apoptosis, but apoptosis does not explain persistent virus-induced cell death. The decision whether autophagy takes a moderate or excess route depends on what pathways are activated during stress, increased mTORC2/p70S6K dependent signaling is a route to excessive activation of apparently overwhelming, lethal, unrestrained autophagy. Whether this regulation is part of a situation called autophagic programmed cell death (Tsujimoto and Shimizu, 2005) remains to be determined. A proportion of cells during infection after apoptosis and autophagy inhibition still die through an unidentified alternative means indicating the redundancy of death mechanisms in cells. The question of other unidentified programs of cell death aside from apoptosis, autophagic death or necroptosis lingers to this day. Regardless of the complexity of cell death, how a shift of autophagy between a protective and a lethal role is controlled, and whether this shift can be influenced, remains a fruitful subject of study.

Materials and methods

Cell culture and treatment

Madin-Darby Canine Kidney (MDCK) (a gift of Dr. Anastasia Gregoriades, Queens College, Flushing, NY), ATG 5 KO mouse embryonic fibroblasts (ATG5 MEF) (a gift of Dr. Patrizia Agostinis, Catholic University of Leuven, Belgium) and MCF7 (ATCC#HTB-22) cells were maintained in Dulbecco's Minimum Essential Media (DMEM) with 10% FBS, 50 U/ml penicillin and 50 mg/ml streptomycin at 37 °C under a 5% CO_2 atmosphere. Final concentration of 5 mM L-glutamine was added to the ATG5 MEF media. Prior to all infections, cells were seeded and allowed to attach overnight in maintenance media. Cells were washed with 1 × Phosphate Buffered Saline (PBS) before infecting at multiplicity of infection (MOI)=5. Sufficient virus was added by diluting virus stock with ice-cold virus diluting media (PBS with 0.2% BSA, 1 mM $MgCl_2$, 0.9 mM $CaCl_2$, 50 U/ml penicillin and 50 mg/ml streptomycin) and adding to cells for 1 h at room temperature. Cells were then washed once with 1 × PBS and covered with DMEM with 5% FBS, and incubated at 37 °C, 5% CO_2 until data collection.

Influenza A virus (A/WSN/33), described below as WSN, was generously provided by Dr. Garcia-Sastre (Mount Sinai Medical School, NY). For expansion of influenza stocks, 10-day-old specific-pathogen-free embryonated chicken eggs (Charles River SPAFAS, North Franklin, CT) were infected with virus and incubated at 35 °C for 2 days. Allantoic fluid from infected eggs was spun at 3000 rpm for 5 min, then stored at −80 °C. Viral titers of influenza stock solutions were determined by plaque assay as described previously (Han et al., 1995). Briefly, monolayers of MDCK cells were incubated overnight in DMEM containing 10% FBS and 1% pen-strep. This was followed by infection with 10-fold serial dilutions of virus suspension for 1 h at room temperature. Cells were then covered with warmed Eagle's minimum essential medium (#12-668E, BioWhittaker) containing 0.1% DEAE–dextran (#D9885, Sigma-Aldrich) and 2% purified agar (#LP0028, Oxoid). This agar medium was allowed to solidify at room temperature and the cells were incubated for 2 days at 37 °C for plaque development. Prior to analysis the solidified agar was removed, and the cells were fixed and stained with a methanol–crystal violet solution. Plaques were counted, and the virus titer was expressed as PFU/ml.

When appropriate, pancaspase inhibitor zVAD-fmk (zVAD) (#BML-P416-0001, Biomol International) was applied at 50 μM final concentration (Lockshin and Zakeri, 2002), class I/III PI3K inhibitor Wortmannin (wort) (#681675, Calbiochem) at 20–40 μM (McLean et al., 2011; Ravikumar et al., 2010), class III PI3K inhibitor 3-methyladenine (3 MA) (#M9281 Sigma) at 5–20 mM (Zhou et al., 2009; McLean et al., 2011; Levine and Kroemer 2008), necroptosis inhibitor necrostatin (lot#F0712, Santa Cruz Biotechnology) at 50–200 μM (Degterev et al., 2005), mTOR inhibitors rapamycin (#R0395, Sigma) at 50 nM (McLean et al., 2011; Levine and Kroemer 2008) and torin1 (#4247, R&D) at 4 or 20 nM (Ravikumar et al., 2010; Liu et al., 2010) and p70S6K inhibitor bis-indolylmaleimide V (p70i) (lot#D00074865, Calbiochem) at 8–100 μM (Marmy-Conus et al., 2002). In these cases, cells were incubated with inhibitors for 1 h prior to infection. Lysosome cathepsin D inhibitor pepstatin A (lot#D00103354, Calbiochem) was added at 10 μg/ml of media after infection (Lockshin and Zakeri 2002; McLean et al., 2011). Inhibition by zVAD (Figs. 3B and C, and 5B), Wortmannin (Fig. 5A–C), 3MA (Fig. 5D), rapamycin (Fig. 7A), torin1 (Fig. 7C) and p70i (Fig. 7E) was experimentally verified.

Assessment of cell viability and death

Cells were infected with influenza A virus at MOI=5. The cells were incubated for 1 h at room temperature, washed once with 1 × PBS and covered with maintenance media at 37 °C, 5% CO_2 and harvested at various times. Infected cells were collected by trypsin digestion, and stained with 0.4% trypan blue in 1 × PBS; exclusion of trypan blue correlates well with other viability assays. Live (white) and dead (blue) cells were counted on a hemocytometer,

with cell viability expressed as percent dead cells above the percent found in mock-infected cultures. Mock-infection is treatment with virus media without virus then addition with new media as an equivalent to 0 HPI or uninfected cells. Experiments were done in triplicate and the Student *T*-test was used to determine significant differences in cell death.

To assess apoptosis, nuclear and DNA fragmentation were determined. DNA fluorochrome bis-benzimide (Hoechst 33258) was used to assess the amount of nuclear fragmentation in infected cells as described previously (McLean et al., 2009). Fragmented nuclei were counted using a Leitz DMRB fluorescence microscope. Nuclei that had fragmented into small dense bodies were considered apoptotic while nuclei with evenly dispersed chromatin were non-apoptotic.

For DNA cleavage cells plated at a density of 7×10^6 cells were infected with virus and collected for DNA extraction at various HPI. After scraping of cells and centrifugation the pellet was resuspended with 0.5 ml lysis buffer (10 mM Tris–HCl at pH 7.5, 10 mM EDTA at pH8.0, and 0.2% Triton X-100) and incubated on ice for 15 min. Lysate was centrifuged at 12,000*g* for 20 min. and the supernatant was treated with 5 ml RNase A (100 μg/ml) and incubated at 37 °C for 1 h. DNA was purified by phenol extractions and precipitated overnight by 2.5 volume of 100% ethanol. Resuspended DNA was run on a 2% agarose gel and viewed with a UV transluminator for detection of DNA laddering (Karasavvas and Zakeri, 1999).

Transmission electron microscopy (TEM)

Reagents were purchased from Electron Microscopy Sciences (Fort Washington, PA). MDCK cells were plated at a density of 1.5×10^6, infected with influenza virus at a MOI of 5 with or without treatment. After 24 HPI, cells were fixed in 2.5% glutaraldehyde in 0.2 M cacodylate buffer, pH 7.4 for 20 min at room temperature (RT) on the plate. Cells were then scraped off and centrifuged in conical tubes at 1200*g* for 5 min. After washing in cacodylate buffer cells were post-fixed with 1% osmium tetroxide in the same buffer for 1 h at RT and washed again. Cells were then dehydrated through ascending ethanol concentrations (50–100%) for 10 min each and embedded in Agar 100 epoxy resin. Sections were counterstained with lead citrate and uranyl acetate. High-resolution images were taken with a Philips 208 electron microscope.

Western blot and cytochemistry

Cells were infected and treated as described above. Western blot analysis was performed as described by Lin et al. (2006). Briefly, treated cells were scraped and washed with ice-cold 1 × PBS before whole cell lysate proteins were collected in RIPA buffer and quantified using the BioRad protein assay and an Ultrospec III spectrophotometer (Pharmacia LKB, Sweden). Western blot analysis was performed by sodium dodecyl sulfate-polyacrylamide gel electrophoresis (SDS-PAGE), using primary antibodies: anti-active caspase 3 (#559565, BD Pharmingen), anti-caspase 3 and anti-cleaved caspase 8 (both graciously given by Donald Nicholson, Merck Frosst, Canada), anti-PARP (# sc7150, Santa Cruz Biotechnology), anti-LC3 (# L7543, Sigma-Aldrich), anti-phosphorylated Akt (#9271S), anti-Akt (#9272S), anti-phosphorylated mTOR (#D9C2), anti-mTOR (#7C10), anti-phosphorylated p70S6K (#108D2), anti-p70S6K (#2708), anti-phosphorylated Erk1/2 (#4377, all from Cell Signaling), anti-Bcl2 (#sc492), and anti-β-tubulin (# sc9104, loading control, both from Santa Cruz), α-tubulin (#t6074, Sigma-Aldrich), and anti-influenza α-NP protein (graciously given by Dr. Adolfo Garcia Sastre, Mount Sinai, NY). Positive signals were detected using ECL (#RPN2132, GE Healthcare) and visualized using an Amersham Hyperfilm ECL photoradiographic film (# 28906835, GE Healthcare) or a Typhoon 9410 Variable mode Imager (GE Healthcare).

Cytochemical analysis was performed as described by Lin et al. (2006). Cells were seeded on flame-sterilized glass cover slips, allowed to attach overnight, infected and treated as above. After treatment 24 HPI, cells were washed with 1 × PBS and fixed with fresh, ice-cold 3% paraformaldehyde for 10 min, washed once and stored in 1 × PBS in dark at 4 °C. Cells were transfected with GFP-LC3 plasmid (provided by Guido Kroemer, Institut Gustave-Roussy, Villejuif, France) using the Lipofectamine 2000 system (# 52887, Invitrogen) according to manufacturer's protocol. Post-transfection, cells were incubated at 37 °C for at least 16 h before collection or treatment to allow plasmid expression. LC3-GFP expressing cells were embedded immediately following fixation. For both situations cells were embedded by Gel Mount (#M-01, Biomeda) and observed by confocal microscopy (Leica, Germany).

For measurements of lysosomal activity, cells were infected and collected as described above. The activity of the lysosomal enzyme acid phosphatase was assessed using an acid phosphatase assay kit (#CS0740, Sigma) according to the manufacturer's protocol and 10^6 cells from each sample. The absorbance of each sample at 405 nm was measured spectrophotometrically with an Ultraspec III spectrophotometer (Pharmacia LKB, Sweden).

Acknowledgment

We thank Dr. Guido Kroemer for providing several plasmids used in our experiments. We give special thanks to Dr. Timothy Short, Fiorella Ortiz-Penaloza, Dr. Areti Tsiola, Dr. Karl Fath, Heather Drake and Narges Zali for providing the technical and editorial support. We also thank the Queens College Core Facility for Imaging, Molecular and Cellular Biology, for access to their facilities.

This work was supported in part by funding from the NIAID NIH Grant 1R15AIO94351-01 to ZZ and the NIH NIGMS (MARC-USTAR) Grant T 34 GM070387.

Appendix. Supporting information

Supplementary data associated with this article can be found in the online version at http://dx.doi.org/10.1016/j.virol.2014.01.008.

References

Abeliovich, H., Dunn , W.A., Kim, J., Klionsky, D.J., 2000. Dissection of autophagosome biogenesis into distinct nucleation and expansion steps. J. Cell Biol. 151, 1025–1034.

Alexander, A., Cai, S.L., Kim, J., Nanez, A., Sahin, M., MacLean, K.H., Inoki, K., Guan, K.L., Shen, J., Person, M.D., Kusewitt, D., Mills, G.B., Kastan, M.B., Walker, C.L., 2010. ATM signals to TSC2 in the cytoplasm to regulate mTORC1 in response to ROS. Proc. Natl. Acad. Sci. USA 107, 4153–4158.

Avni, D., Shama, S., Loreni, F., Meyuhas, O., 1994. Vertebrate mRNAs with a 5′-terminal pyrimidine tract are candidates for translational repression in quiescent cells: characterization of the translational cis-regulatory element. Mol. Cell. Biol. 14, 3822–3833.

Aweya, J.J., Mak, T.M., Lim, S.G., Tan, Y.J., 2013. The p7 protein of the hepatitis C virus induces cell death differently from the influenza A virus viroporin M2. Virus Res. 172, 24–34.

Chang, Y.Y., Juhasz, G., Goraksha-Hicks, P., Arsham, A.M., Mallin, D.R., Muller, L.K., Neufeld, T.P., 2009. Nutrient-dependent regulation of autophagy through the target of rapamycin pathway. Biochem. Soc. Trans. 37, 232–236.

Chen, W., Calvo, P.A., Malide, D., Gibbs, J., Schubert, U., Bacik, I., Basta, S., O'Neill, R., Schickli, J., Palese, P., Henklein, P., Bennink, J.R., Yewdell, J.W., 2001. A novel influenza A virus mitochondrial protein that induces cell death. Nat. Med. 7, 1306–1312.

Corradetti, M., Guan, K., 2006. Upstream of the mammalian target of rapamycin: do all roads pass through mTOR? Oncogene 25, 6347–6360.

Degterev, A., Huang, Z., Boyce, M., Li, Y., Jagtap, P., Mizushima, N., Cuny, G.D., Mitchison, T.J., Moskowitz, M.A., Yuan, J., 2005. Chemical inhibitor of non-apoptotic cell death with therapeutic potential for ischemic brain injury. Nat. Chem. Biol. 1, 112–119.

Feldman, M.E., Apsel, B., Uotila, A., Loewith, R., Knight, Z.A., Ruggero, D., Shokat, K.M., 2009. Active-site inhibitors of mTOR target rapamycin-resistant outputs of mTORC1 and mTORC2. PLoS Biol.7, e38.
Gannage, M., Dormann, D., Albrecht, R., Dengjel, J., Torossi, T., Ramer, P.C., Lee, M., Strowig, T., Arrey, F., Conenello, G., Pypaert, M., Andersen, J., Garcia-Sastre, A., Munz, C., 2009. Matrix protein 2 of influenza A virus blocks autophagosome fusion with lysosomes. Cell Host Microbe6, 367–380.
Gill, J.R., Sheng, Z.M., Ely, S.F., Guinee, D.G., Beasley, M.B., Suh, J., Deshpande, C., Mollura, D.J., Morens, D.M., Bray, M., Travis, W.D., Taubenberger, J.K., 2010. Pulmonary pathologic findings of fatal 2009 pandemic influenza A/H1N1 viral infections. Arch. Pathol. Lab. Med. 134, 235–243.
Hale, B.G., Jackson, D., Chen, Y.H., Lamb, R.A., Randall, R.E., 2006. Influenza A virus NS1 protein binds p85beta and activates phosphatidylinositol-3-kinase signaling. Proc. Natl. Acad. Sci. USA 103, 14194–14199.
Han, J.W., Pearson, R.B., Dennis, P.B., Thomas, G., 1995. Rapamycin, wortmannin, and the methylxanthine SQ20006 inactivate p70s6k by inducing dephosphorylation of the same subset of sites. J. Biol. Chem. 270, 21396–21403.
Ilyinskii, P.O., Gambaryan, A.S., Meriin, A.B., Gabai, V., Kartashov, A., Thoidis, G., Shneider, A.M., 2008. Inhibition of influenza M2-induced cell death alleviates its negative contribution to vaccination efficiency. PLoS One 3, e1417.
Ito, T., Kobayashi, Y., Morita, T., Horimoto, T., Kawaoka, Y., 2002. Virulent influenza A viruses induce apoptosis in chickens. Virus Res. 84, 27–35.
Jefferies, H.B., Fumagalli, S., Dennis, P.B., Reinhard, C., Pearson, R.B., Thomas, G., 1997. Rapamycin suppresses 5′TOP mRNA translation through inhibition of p70s6k. EMBO J. 16, 3693–3704.
Jiang, B.H., Liu, L.Z., 2008. PI3K/PTEN signaling in tumorigenesis and angiogenesis. Biochim. Biophys. Acta (BBA) – Proteins Proteomics 1784, 150–158.
Karasavvas, N., Zakeri, Z., 1999. Relationships of apoptotic signaling mediated by ceramide and TNF-alpha in U937 cells. Cell Death Differ. 6, 115–123.
Kim, K.W., Mutter, R.W., Cao, C., Albert, J.M., Freeman, M., Hallahan, D.E., Lu, B., 2006. Autophagy for cancer therapy through inhibition of pro-apoptotic proteins and mammalian target of rapamycin signaling. J. of Biol. Chem. 281, 36883–36890.
Lawrence, B.P., Brown, W.J., 1993. Inhibition of protein synthesis separates autophagic sequestration from the delivery of lysosomal enzymes. J. Cell Sci. 105 (Pt. 2), 73-–80..
Lazareno, S., Popham, A., Birdsall, N.J., 1998. Muscarinic interactions of bisindolylmaleimide analogues. Eur. J. Pharmacol. 360, 281–284.
Levine, B., Kroemer, G., 2008. Autophagy in the pathogenesis of disease. Cell 132, 27–42.
Levy, S., Avni, D., Hariharan, N., Perry, R.P., Meyuhas, O., 1991. Oligopyrimidine tract at the 5′ end of mammalian ribosomal protein mRNAs is required for their translational control. Proc. Natl. Acad. Sci. USA 88, 3319–3323.
Lin, L., Ye, Y., Zakeri, Z., 2006. p53, Apaf-1, caspase-3, and -9 are dispensable for Cdk5 activation during cell death. Cell Death Differ. 13, 141–150.
Liu, Q., Chang, J.W., Wang, J., Kang, S.A., Thoreen, C.C., Markhard, A., Hur, W., Zhang, J., Sim, T., Sabatini, D.M., Gray, N.S., 2010. Discovery of 1-(4-(4-propionylpiperazin-1-yl)-3-(trifluoromethyl)phenyl)-9-(quinolin-3-yl)benz o[h][1,6]naphthyridin-2 (1H)-one as a highly potent, selective mammalian target of rapamycin (mTOR) inhibitor for the treatment of cancer. J. Med. Chem. 53, 7146–7155.
Lockshin, R.A., Zakeri, Z., 2002. Caspase-independent cell deaths. Curr. Opin. Cell Biol.14, 727–733.
Marmy-Conus, N., Hannan, K.M., Pearson, R.B., 2002. Ro 31-6045, the inactive analogue of the protein kinase C inhibitor Ro 31-8220, blocks in vivo activation of p70(s6k)/p85(s6k): implications for the analysis of S6K signalling. FEBS Lett.519, 135–140.
McLean, J.E., Datan, E., Matassov, D., Zakeri, Z.F., 2009. Lack of Bax prevents influenza A virus-induced apoptosis and causes diminished viral replication. J. Virol. 83, 8233–8246.
McLean, J.E., Wudzinska, A., Datan, E., Quaglino, D., Zakeri, Z., 2011. Flavivirus NS4A-induced autophagy protects cells against death and enhances virus replication. J. Biol. Chem. 286, 22147.
Meyer, L.R., Zweig, A.S., Hinrichs, A.S., Karolchik, D., Kuhn, R.M., Wong, M., Sloan, C.A., Rosenbloom, K.R., Roe, G., Rhead, B., Raney, B.J., Pohl, A., Malladi, V.S., Li, C.H., Lee, B.T., Learned, K., Kirkup, V., Hsu, F., Heitner, S., Harte, R.A., Haeussler, M., Guruvadoo, L., Goldman, M., Giardine, B.M., Fujita, P.A., Dreszer, T.R., Diekhans, M., Cline, M.S., Clawson, H., Barber, G.P., Haussler, D., Kent, W.J., 2013. The UCSC Genome Browser database: extensions and updates 2013. Nucleic Acids Res. 41, D64–D69.
Mizushima, N., Yoshimori, T., Levine, B., 2010. Methods in mammalian autophagy research. Cell 140, 313–326.
Mohsin, M.A., Morris, S.J., Smith, H., Sweet, C., 2002. Correlation between levels of apoptosis, levels of infection and haemagglutinin receptor binding interaction of various subtypes of influenza virus: does the viral neuraminidase have a role in these associations. Virus Res. 85, 123–131.
Mori, I., Komatsu, T., Takeuchi, K., Nakakuki, K., Sudo, M., Kimura, Y., 1995. In vivo induction of apoptosis by influenza virus. J. Gen. Virol. 76, 2869.
Morris, S.J., Price, G.E., Barnett, J.M., Hiscox, S.A., Smith, H., Sweet, C., 1999. Role of neuraminidase in influenza virus-induced apoptosis. J. Gen. Virol. 80 (Pt. 1), 137–146.
Nencioni, L., De Chiara, G., Sgarbanti, R., Amatore, D., Aquilano, K., Marcocci, M.E., Serafino, A., Torcia, M., Cozzolino, F., Ciriolo, M.R., Garaci, E., Palamara, A.T., 2009. Bcl-2 expression and p38MAPK activity in cells infected with influenza A virus: impact on virally induced apoptosis and viral replication. J. Biol. Chem. 284, 16004–16015.
Nicklin, P., Bergman, P., Zhang, B., Triantafellow, E., Wang, H., Nyfeler, B., Yang, H., Hild, M., Kung, C., Wilson, C., Myer, V.E., MacKeigan, J.P., Porter, J.A., Wang, Y.K., Cantley, L.C., Finan, P.M., Murphy, L.O., 2009. Bidirectional transport of amino acids regulates mTOR and autophagy. Cell 136, 521–534.
Olsen, C.W., Kehren, J.C., Dybdahl-Sissoko, N.R., Hinshaw, V.S., 1996. bcl-2 alters influenza virus yield, spread, and hemagglutinin glycosylation. J. Virol. 70, 663–666.
Pastor, M.D., Garcia-Yebenes, I., Fradejas, N., Perez-Ortiz, J.M., Mora-Lee, S., Tranque, P., Moro, M.A., Pende, M., Calvo, S., 2009. mTOR/S6 kinase pathway contributes to astrocyte survival during ischemia. J. Biol. Chem. 284, 22067–22078.
Pattingre, S., Espert, L., Biard-Piechaczyk, M., Codogno, P., 2008. Regulation of macroautophagy by mTOR and Beclin 1 complexes. Biochimie 90, 313–323.
Ravikumar, B., Sarkar, S., Davies, J.E., Futter, M., Garcia-Arencibia, M., Green-Thompson, Z.W., Jimenez-Sanchez, M., Korolchuk, V.I., Lichtenberg, M., Luo, S., Massey, D.C., Menzies, F.M., Moreau, K., Narayanan, U., Renna, M., Siddiqi, F.H., Underwood, B.R., Winslow, A.R., Rubinsztein, D.C., 2010. Regulation of mammalian autophagy in physiology and pathophysiology. Physiol. Rev. 90, 1383–1435.
Scott, R.C., Schuldiner, O., Neufeld, T.P., 2004. Role and regulation of starvation-induced autophagy in the Drosophila fat body. Dev. Cell 7, 167–178.
Sekulic, A., Hudson, C.C., Homme, J.L., Yin, P., Otterness, D.M., Karnitz, L.M., Abraham, R.T., 2000. A direct linkage between the phosphoinositide 3-kinase-AKT signaling pathway and the mammalian target of rapamycin in mitogen-stimulated and transformed cells. Cancer Res. 60, 3504–3513.
Setalo , G., Singh, M., Nethrapalli, I.S., Toran-Allerand, C.D., 2005. Protein kinase C activity is necessary for estrogen-induced Erk phosphorylation in neocortical explants. Neurochem. Res. 30, 779–790.
Suh, Y., Afaq, F., Khan, N., Johnson, J.J., Khusro, F.H., Mukhtar, H., 2010. Fisetin induces autophagic cell death through suppression of mTOR signaling pathway in prostate cancer cells. Carcinogenesis 31, 1424–1433.
Tanida, I., Minematsu-Ikeguchi, N., Ueno, T., Kominami, E., 2005. Lysosomal turnover, but not a cellular level, of endogenous LC3 is a marker for autophagy. Autophagy 1, 84–91.
Taubenberger, J.K., Morens, D.M., 2008. The pathology of influenza virus infections. Annu. Rev. Pathol. 3, 499–522.
Tripathi, S., Batra, J., Cao, W., Sharma, K., Patel, J.R., Ranjan, P., Kumar, A., Katz, J.M., Cox, N.J., Lal, R.B., Sambhara, S., Lal, S.K., 2013. Influenza A virus nucleoprotein induces apoptosis in human airway epithelial cells: implications of a novel interaction between nucleoprotein and host protein Clusterin. Cell Death Dis.4, e562.
Tsujimoto, Y., Shimizu, S., 2005. Another way to die: autophagic programmed cell death. Cell Death Differ. 12 (Suppl. 2), S1528–S1534.
Vanhaesebroeck, B., Alessi, D.R., 2000. The PI3K-PDK1 connection: more than just a road to PKB. Biochem. J. 346 (Pt. 3), 561–576.
White, E., 2008. Autophagic cell death unraveled: pharmacological inhibition of apoptosis and autophagy enables necrosis. Autophagy 4, 399–401.
Widjaja, I., de Vries, E., Rottier, P.J., de Haan, C.A., 2012. Competition between influenza A virus genome segments. PLoS One 7, e47529.
Wong, C.H., Iskandar, K.B., Yadav, S.K., Hirpara, J.L., Loh, T., Pervaiz, S., 2010. Simultaneous induction of non-canonical autophagy and apoptosis in cancer cells by ROS-dependent ERK and JNK activation. PLoS One 5, e9996.
Wu, Y.T., Tan, H.L., Huang, Q., Kim, Y.S., Pan, N., Ong, W.Y., Liu, Z.G., Ong, C.N., Shen, H.M., 2008. Autophagy plays a protective role during zVAD-induced necrotic cell death. Autophagy 4, 457–466.
Wurzer, W.J., Planz, O., Ehrhardt, C., Giner, M., Silberzahn, T., Pleschka, S., Ludwig, S., 2003. Caspase 3 activation is essential for efficient influenza virus propagation. EMBO J. 22, 2717–2728.
Wurzer, W.J., Ehrhardt, C., Pleschka, S., Berberich-Siebelt, F., Wolff, T., Walczak, H., Planz, O., Ludwig, S., 2004. NF-kappaB-dependent induction of tumor necrosis factor-related apoptosis-inducing ligand (TRAIL) and Fas/FasL is crucial for efficient influenza virus propagation. J. Biol. Chem. 279, 30931–30937.
Yamashita, R., Suzuki, Y., Takeuchi, N., Wakaguri, H., Ueda, T., Sugano, S., Nakai, K., 2008. Comprehensive detection of human terminal oligo-pyrimidine (TOP) genes and analysis of their characteristics. Nucleic Acids Res. 36, 3707–3715.
Yang, J.C., Chien, C.T., 2009. A new approach for the prevention and treatment of Helicobacter pylori infection via upregulation of autophagy and downregulation of apoptosis. Autophagy 5, 413–414.
Yorimitsu, T, Klionsky, DJ., 2005. Autophagy: molecular machinery for self-eating. Cell death Differ. 12 (Suppl. 2), S1542–S1552.
Zakeri, Z., Lockshin, R.A., Criado-Rodriguez, L.M., Martinez, A.C., 2005. A generalized caspase inhibitor disrupts early mammalian development. Int. J. Dev. Biol. 49, 43–47.
Zamarin, D., Garcia-Sastre, A., Xiao, X., Wang, R., Palese, P., 2005. Influenza virus PB1-F2 protein induces cell death through mitochondrial ANT3 and VDAC1. PLoS Pathog. 1, e4.
Zhang, C., Yang, Y., Zhou, X., Liu, X., Song, H., He, Y., Huang, P., 2010. Highly pathogenic avian influenza A virus H5N1 NS1 protein induces caspase-dependent apoptosis in human alveolar basal epithelial cells. Virol. J. 7, 51.
Zhirnov, O.P., Klenk, H.D., 2009. Alterations in caspase cleavage motifs of NP and M2 proteins attenuate virulence of a highly pathogenic avian influenza virus. Virology 394, 57–63.
Zhirnov, O.P., Konakova, T.E., Garten, W., Klenk, H., 1999. Caspase-dependent N-terminal cleavage of influenza virus nucleocapsid protein in infected cells. J. Virol. 73, 10158–10163.
Zhou, Z., Jiang, X., Liu, D., Fan, Z., Hu, X., Yan, J., Wang, M., Gao, G.F., 2009. Autophagy is involved in influenza A virus replication. Autophagy 5, 321–328.